HHS Public Access

Author manuscript

FASEB J. Author manuscript; available in PMC 2020 October 28.

Published in final edited form as:

FASEB J. 2020 January ; 34(1): 1211–1230. doi:10.1096/fj.201901888R.

Novel molecular mechanisms for Prph2-associated pattern dystrophy

Dibyendu Chakraborty[1,2], **Daniel G. Strayve**[1], **Mustafa S. Makia**[1], **Shannon M. Conley**[2], **Mashal Kakahel**[1], **Muayyad R. Al-Ubaidi**[1], **Muna I. Naash**[1]

[1]Department of Biomedical Engineering, University of Houston, Houston, TX, USA

[2]Department of Cell Biology, University of Oklahoma Health Sciences Center, Oklahoma City, OK, USA

Abstract

Mutations in peripherin 2 (*PRPH2*) have been associated with retinitis pigmentosa (RP) and macular/pattern dystrophies, but the origin of this phenotypic variability is unclear. The majority of Prph2 mutations are located in the large intradiscal loop (D2), a region that contains seven cysteines involved in intra- and intermolecular disulfide bonding and protein folding. A mutation at cysteine 213, which is engaged in an intramolecular disulfide bond, leads to butterfly-shaped pattern dystrophy in humans, in sharp contrast to mutations in the adjacent cysteine at position 214 which result in RP. To help understand this unexpected phenotypic variability, we generated a knockin mouse line carrying the C213Y disease mutation. The mutant Prph2 protein lost the ability to oligomerize with rod outer segment membrane protein 1 (Rom1), but retained the ability to form homotetramers. C213Y heterozygotes had significantly decreased overall Prph2 levels as well as decreased rod and cone function. Critically, supplementation with extra wild-type Prph2 protein elicited improvements in Prph2 protein levels and rod outer segment structure, but not functional rescue in rods or cones. These findings suggest that not all interruptions of D2 loop intramolecular disulfide bonding lead to haploinsufficiency-related RP, but rather that more subtle changes can lead to mutant proteins stable enough to exert gain-of-function defects in rods and cones. This outcome highlights the difficulty in targeting Prph2-associated gain-of-function disease and suggests that elimination of the mutant protein will be a pre-requisite for any curative therapeutic strategy.

Correspondence Muayyad R. Al-Ubaidi and Muna I. Naash, Department of Biomedical Engineering, University of Houston, 3517 Cullen Blvd. SERC 2009, Houston, TX 77204-5060, USA. malubaid@Central.UH.EDU (M. R. A.-U.), mnaash@central.uh.edu (M. I. N.).

Present address

Dibyendu Chakraborty, Department of Ophthalmology, University of Alabama at Birmingham, Birmingham, AL 35294, USA

AUTHOR CONTRIBUTIONS

D. Chakraborty, S.M. Conley, M.R. Al-Ubaidi, and M.I. Naash designed the experiments; D. Chakraborty, D.G. Strayve, and M.S. Makia performed the experiments. All authors participated in analyzing experiments. D. Chakraborty and D.G. Strayve wrote the original version of the manuscript. All authors edited and approved the manuscript.

CONFLICT OF INTEREST

The authors declare that they have no conflicts of interest.

Keywords

butterfly pattern dystrophy; C213Y knockin; disulfide linkages; extracellular loop; retinitis pigmentosa; retinal degeneration slow (RDS); tetraspanin

1 | INTRODUCTION

Peripherin 2 (Prph2, also known as rds) is a photoreceptor-specific tetraspanin protein localized to the disc rim of rod and cone outer segments (OSs). Mutations in *PRPH2* are associated with a variety of autosomal dominant retinal degenerative diseases, including retinitis pigmentosa (RP), cone-rod dystrophy, and multiple forms of macular dystrophy (http://www.retina-international.org/files/sci-news/rdsmut.htm).[1] No treatments for these diseases currently exist, and progress developing therapeutics has been hampered by several factors. First, both rods and cones express Prph2 but are affected distinctly by different *PRPH2* mutations and secondary defects can occur in adjacent tissues such as the retinal pigment epithelium (RPE) and choroid. Second, multiple different, possibly overlapping, disease mechanisms exist, and they are, as yet, incompletely understood. Third, there is vast variability in clinical phenotype, diagnosis, age of onset, severity, and penetrance, often within families carrying the same mutation. This complicates correlations with animal models and suggests that additional modifying factors (such as modifier genes or the presence of nonpathogenic Prph2/Rom1 variants) may play a role in some cases.[2–4] Finally, the retina is severely affected by Prph2 haploinsufficiency, so levels of expression must be carefully titrated to generate rescue (eg, with gene therapy), and in animal models with variable levels of expression, it can be difficult to separate the effects of haploinsufficiency from the effects of the mutation.[5–8] In spite of these challenges, we and others have identified key structural regions of the Prph2 protein such as the second intradiscal (D2) loop,[9,10] and begun to develop an understanding of Prph2 disease processes tied to the effects of mutations on these key regions.

Prph2 is necessary for the formation of OSs, and specifically the disc/lamellae rim region. *Prph2*$^{-/-}$ mouse retinas completely fail to develop OS structures[11]; and haploinsufficiency in the *Prph2*$^{+/-}$ retina leads to disorganized OSs with malformed discs and rod-dominant defects in retinal function.[5] Prph2 forms noncovalent homo- and hetero-tetramers with its non-glycosylated homologue, rod outer segment membrane protein 1 (Rom1),[12] which then assemble into covalently linked larger complexes. The region of interaction between Prph2-Prph2 and Prph2-Rom1 has been mapped to the D2 loop of Prph2,[9] and the presence of a disproportionately high number of pathogenic mutations in this region supports it as a key player in Prph2 function. The D2 loop contains seven highly conserved cysteine (Cys) residues, of which six are involved in intramolecular disulfide bonds.[13] The seventh, Cys150, forms the intermolecular disulfide bonds responsible for assembly of large Prph2 oligomers. In models where Cys150-mediated intermolecular bonding is impaired and there are no large Prph2 complexes, for example in the *Prph2*$^{C150S/C150S}$ knockin or in a similar model in which a nearby lysine is deleted (*Prph2*$^{K153del/K153del}$), no OSs form.[14–16] Animals heterozygous for these pathogenic Prph2 mutations (which mimic the autosomal dominant inheritance pattern in patients) develop cone-rod or cone-dominant phenotypes associated

with gain-of-function and dominant negative effects. In contrast, our previous experiments as well as patient phenotypes suggest that eradicating intramolecular disulfide bonding in the D2 loop, for example in the C214S mutant, leads to pure haploinsufficiency.[8] This causes a rod-dominant defect (similar to that seen in the *Prph2*$^{+/-}$ mice) and RP in patients,[17] with secondary cone defects appearing only much later.

However, recent evidence suggests that this dichotomous understanding of Prph2-associated disease wherein rod-dominant disease is caused by haploinsufficiency-associated mutations, while cone-rod and macular dystrophies are associated with mutants that abnormally affect Prph2 oligomerization may be overly simplistic. For example, while mutations that affect Prph2 intermolecular bonding such as K153del and Y141C do cause macular/pattern dystrophies in patients (consistent with the cone-rod phenotype in animal models[2,14,18]), they can also cause RP.[19,20] In addition, while the intramolecular disulfide bonding mutant C214S causes rod-dominant RP in patients and animal models,[8,17] other mutations in D2 loop cysteines associated with intramolecular bonding, such as C213Y, do not cause rod-dominant RP, but rather butterfly pattern dystrophy/macular dystrophy.[1,21–23] This inconsistency in patient phenotypes among mutations predicted to exert similar effects strongly suggests that complex disease mechanisms remain to be elucidated. Here, our goal was to help expand our understanding of Prph2 disease by evaluating the molecular mechanisms associated with the C213Y Prph2 mutation using a knockin mouse model. We observe that, in contrast to C214S-mediated haploinsufficiency, C213Y Prph2 exhibits a dominant negative effect on both rods and cones. This phenotype is accompanied by severe defects in Prph2/Rom1 oligomerization and trafficking, and cannot be rescued by supplementation with excess wild-type (WT) Prph2.

2 | MATERIALS AND METHODS

2.1 | Animal care and use

Animal maintenance and experiments were approved by the local Institutional Animal Care and Use Committee (IACUC; University of Houston, TX, USA) and guidelines as stated by the Association for Research in Vision and Ophthalmology (Rockville, MD). The C213Y-*Prph2* knockin mice were generated by inGenious Targeting Laboratory, Inc (Ronkonkoma, NY, USA). The knockin was made using the same approach as previously described.[18,24] An 8.21 kb fragment used to construct the targeting vector was first sub cloned from a positively identified C57BL/6 BAC clone (RP23: 68M9). The region was designed such that the long homology arm (LA) extends 5.29 kb 5′ to the first point mutation (TGC → TAC) in exon 2 and the LoxP/FRT flanked Neo cassette is inserted 882 bp 3′ to the second point mutation (CCG → CCA) engineered into exon 2. The second point mutation is silent and introduces a restriction site to facilitate genotyping. The short homology arm (SA) extends 2.02 kb 3′ to the LoxP flanked Neo cassette. The targeting vector was constructed using Red/ET recombineering technology. The BAC was sub cloned into a ~2.4 kb backbone vector (pSP72, Promega, Madison, and Wikipedia) containing an ampicillin selection cassette for retransformation of the construct prior to electroporation. A pGK-gb2 loxP/FRT Neo cassette was inserted into the gene as described in the project schematic (Figure 1A). The targeting construct was linearized using NotI prior to electroporation into embryonic stem

cells. The total size of the targeting construct (including vector backbone and Neo cassette) is 12.4 kb. Chimeric founders were bred to identify mice with germ line transmission, and they were then bred to FLPeR expressing mice (Stock#003946, Jackson Labs, Bar Harbor, ME, USA) to remove the Neo cassette. PCR genotyping confirmed that these mice do not carry the *rd8* mutation. *Prph2*$^{+/+}$ (WT), *Prph2*$^{+/-}$, and *Prph2*$^{-/-}$ (also known as the *Prph2*$^{rds/rds}$, *rd2,* or *rds* mouse) littermates were used as controls after confirming that WT littermates from heterozygous knockin crosses exhibited similar retinal structure and function to the *Prph2*$^{+/+}$ animals in our colony. Some experiments utilized the previously characterized normal mouse Prph2 (NMP) transgenic mouse in which WT Prph2 is overexpressed in photoreceptors by an IRBP-driven promoter.[25] All animals were maintained in cyclic light (12 hours light, 12 hours dark, ~30 lux).

2.2 | Antibodies

Various primary antibodies that were used for immunoblotting, immunofluorescence, and immuno-gold EM are summarized in Table 1.

2.3 | RNA preparation and analysis

Total RNA was isolated from three different pairs of retinas for each of the indicated genotypes. In brief, retinas were harvested from P30 mice and placed in TRIzol reagent (Life Technologies/ThermoFisher, Waltham, MA, USA). For experiments where thapsigargin was used as a positive control to induce endoplasmic reticulum (ER) stress; retinas were harvested from P30 WT mice, and incubated at 37°C in Dulbecco's Modified Eagle Medium supplemented with 10% fetal bovine serum and 5 μM thapsigargin. After six hours, RNA was harvested as for all other experiments. After placing in trizol, retinas were subjected to mechanical digestion. This suspension was allowed to sit at room temperature for roughly 5 minutes, emulsified with chloroform, and centrifuged in order to extract the total RNA. Total RNA was then further purified using the RNeasy Mini Kit (Qiagen, Inc, Germantown, MD, USA) according to the manufacturer's instructions. qRT-PCR primers were designed to span the introns of the indicated genes, thus eliminating the potential for genomic DNA contamination. RT-PCR reactions were prepared using the SuperScript III One-Step qRT-PCR Kit (Invitrogen), and RT-PCR was performed using the qTOW-ER^{3}G (Analytik Jena) with analysis carried out using qPCRsoft3.4 software. Relative expression was calculated as $2^{-\Delta Ct}$ where $\Delta Ct = Ct_{\text{gene of interest}} - Ct_{\text{ref}}$). Hypoxanthine phosphoribosyltransferase, was used as a reference housekeeping gene. At least three biological replicates were used for each genotype. The primers used are summarized in Table 2.

2.4 | Immunoblot analysis, immunoprecipitation, and velocity sedimentation

Immunoblot, immunoprecipitation, and velocity sedimentation were performed as described previously.[16,26] Retinal extracts were solubilized in 100 μL of chilled (4°C) buffer [PBS pH 7.0 containing 1% triton-X 100, 5 mM EDTA, 5 mg/mL n-ethylmaleimide (NEM), and a standard protease inhibitor cocktail] per retina. Immunoprecipitation was performed using protein A beads and 100 μg protein extract per sample. SDS-PAGE and immunoblotting were performed using standard protocols under reducing conditions (with dithiothreitol [DTT]) or nonreducing conditions (without DTT). Nonreducing velocity sedimentation was

performed using continuous density gradients of 5%−20% sucrose and 200 μg protein/sample. Blots were imaged using a ChemiDoc MP imaging system (Bio-Rad, Temecula, CA).

Densitometric quantification was performed on non-saturated blots using the Image Lab Software (Bio-Rad, Temecula, CA). In some cases brightness was adjusted in figures to enable visualization of hard to see bands. For each quantitative immunoblot experiment (westerns and velocity sedimentation), experiments were repeated on at least 4–8 samples. Each sample represents a single (unpooled) retina coming from separate animal (ie, not two retinas from the same animal). For each experiment, samples were drawn from at least 4–8 separate litters.

2.5 | Electroretinography

Full-field electroretinography (ERG) tests were performed as previously described.[8,27] Mice were dark adapted overnight prior to ERG. Subsequently, animals were anesthetized and eyes were dilated. ERGs were recorded with a UTAS system (LKC, Gaithersburg, MD, USA). Scotopic ERGs were recorded with a strobe flash stimulus of 157 cd-s/m^2 presented to the dark adapted mouse followed by light adaptation for 5 minutes at 29.03 cd/m^2. Photopic responses were recorded from 25 averaged flashes at 157 cd-s/m^2 for white light, 12.5 cd-s/m^2 for green light (530 nm), and 0.79 cd-s/m^2 for UV light (365 nm).

2.6 | Light and transmission electron microscopy

The methods used for tissue collection, processing, plastic-embedding, and transmission electron microscopy (TEM) were described previously.[8,27] Light microscopy was performed using 0.75 μm plastic embedded sections stained with toluidine blue and images were captured at 20× and 40× magnification using a Zeiss microscope. To evaluate outer nuclear layer (ONL) thickness and photoreceptor outer segment (OS) length, images were captured from central superior and inferior regions containing the optic nerve head and at least three retinal sections from three different eyes per genotype were used. ONL and OS layer thickness were measured using Adobe Photoshop CS5. Thin sections (600–800 Å) collected on copper 75/300 mesh grids were then stained with 2% uranyl acetate and Reynolds' lead citrate for TEM. TEM images were collected using a JEOL 100CX electron microscope at an accelerating voltage of 60 kV.

2.7 | Fundus imaging and fluorescein angiography

Fundus imaging and fluorescein angiography were performed using the Micron IV system (Phoenix Research Laboratories, Pleasanton, CA, USA) as previously described.[28] Bright field fundus images and fundus auto fluorescence images were collected first (from anesthetized/dilated animals) and then animals were injected intraperitoneally with 100 μL of 1% (w/v) fluorescein sodium (Sigma-Aldrich, St. Louis, MO). Fluorescein angiography images were captured using GFP filter. All images were captured using StreamPix software (Phoenix Research Labs).

2.8 | Immunofluorescence labeling

Eyes were harvested, dissected, fixed, embedded, and immunostained as previously described for paraffin sectioning,[16] or cryosectioning.[29] Primary antibodies used for immunostaining are described in Table 1. Appropriate AlexaFluor conjugated secondary antibodies (Life Technologies/ThermoFisher) were used at a dilution of 1:1000. Images were captured on a ZEISS Confocal LSM 900 microscope equipped with a Zeiss Axiocam (Zeiss, Jena, Germany) using a 63× (oil, 1.4 NA) objective. Images were then processed using ZEN Image Analysis software (Zeiss, Jena, Germany). All images shown are orthogonally projected from a eight slice confocal *z*-stack.

2.9 | Statistical analysis

Differences between genotypes were analyzed by one-way ANOVA with Tukey's post-hoc comparisons or two-tailed Student's *t*-test (where only two groups were analyzed). Analysis was done using GraphPad Prism version 7.4 (GraphPad Software, La Jolla, CA). Significance was set at $P < .05$. Throughout the manuscript $*P < .05$, $**P < .01$, $***P < .001$ and $****P < .0001$ for indicated pairwise comparisons.

3 | RESULTS

3.1 | C213Y Prph2 protein is expressed at low levels

To conduct our studies on disease mechanisms associated with defects in Prph2 intramolecular disulfide bonding and to avoid the side effects associated with random integration of a transgene, we employed a knockin strategy for the introduction of the C213Y mutation in the *Prph2* gene (Figure 1A). For simplicity, animals carrying the C213Y *Prph2* allele are referred to as $Prph2^{C/+}$ and $Prph2^{C/C}$, for heterozygous and homozygous, respectively. Heterozygous mice genetically mimic patients, carrying one WT and one mutant allele, making them the essential disease model. However, we also evaluated $Prph2^{C/C}$ retinas to directly study the characteristics and capabilities of the mutant protein. Controls included mice carrying the naturally occurring *Prph2* null allele ($Prph2^{rds/rds}$) referred to as $Prph2^{-/-}$ and $Prph2^{+/-}$, as well as $Prph2^{+/+}$ (referred to as WT).

To evaluate the levels of expression of the C213Y allele at the message and protein levels, qRT-PCR and immunoblots were performed on retinas from postnatal (P) day 30 WT and $Prph2^{C/C}$. No differences were found in the levels of *Prph2* transcripts in $Prph2^{C/C}$ retinas compared to WT, consistent with introduction of the C213Y mutation into the native *Prph2* locus (Figure 1B, liver is shown as a negative control for *Prph2* expression). However, though transcript levels were normal, $Prph2^{C/C}$ retinas had only ~10% of WT levels of Prph2 protein (Figure 1C). The levels of Rom1 protein were similarly reduced in $Prph2^{C/C}$ to ~5% of WT (Figure 1D). $Prph2^{C/+}$ retinas had ~50% of WT Prph2 protein levels, and were comparable to those found in the $Prph2^{+/-}$ (Figure 1C), suggesting that C213Y protein is unstable and/or that it adversely affects the stability of WT Prph2. Rom1 levels in the $Prph2^{C/+}$ retinal extracts were ~60% of WT, higher than those in the $Prph2^{+/-}$ (~50% of WT, Figure 1D), though the difference between $Prph2^{+/-}$ and $Prph2^{C/+}$ was not statistically significant. Prph2 usually appears as a doublet, and we and others have hypothesized that the upper band is newly synthesized Prph2 while the bottom band represents a mature form,

though the differences between the two forms have been elusive. In the *Prph2*$^{C/C}$ the upper band predominates, although both bands can be seen in some cases (eg, Figure 2B).

Asn229 in the Prph2 D2 loop is glycosylated and to determine whether the C213Y mutation impaired this glycosylation, retinal extracts were treated with peptide-N-glycosidase (PNGase), an enzyme that cleaves all N-linked glycans. In addition to *Prph2*$^{C/C}$ and WT retinas, we included extracts from our non-glycosylated Prph2 knockin (N229S, *Prph2*$^{N/N24}$) as a control. PNGase treatment downshifted Prph2 bands on immunoblots from WT and *Prph2*$^{C/C}$ retinas (Figure 1E), indicating that the mutant protein is glycosylated. As expected, PNGase treatment did not affect non-glycosylated Rom1. Combined, these findings suggest that the C213Y mutation likely leads to unstable Prph2 protein without blocking Prph2 glycosylation.

3.2 | C213Y Prph2 is unable to bind Rom1 or form high-order molecular weight complexes necessary for OS elaboration

Prph2 and Rom1 function as oligomers, so we performed a series of experiments to probe Prph2/Rom1 complex assembly in the mutant. First, co-immunoprecipitation (co-IP) was performed under nonreducing conditions on retinal extracts from P30 WT and *Prph2*$^{C/C}$ mice using antibodies against the Prph2 and Rom1 C-termini (Figure 2A, top and bottom, respectively). In contrast to WT Prph2, no interaction was detected between C213Y Prph2 and Rom1. In addition, a smaller fraction of total C213Y Prph2 was pulled down with anti-Prph2 compared to WT, suggesting that the mutation also reduced homomeric interactions between Prph2 molecules.

While initially Prph2 and Rom1 assemble into noncovalent homomeric and heteromeric tetramers,[13,26,30] upon localization to OS disc rims, the majority of Prph2 either assembles into higher order homomeric or intermediate heteromeric complexes[26] held together by C150-mediated intermolecular disulfide bonds. Under nonreducing but denaturing conditions, these intermolecular disulfide-linked complexes migrate as dimers at roughly 75 kDa. To evaluate the mutant protein's ability to form covalently linked complexes, we immunoblotted retinal extracts under nonreducing conditions for Prph2 and Rom1 (Figure 2B). Both dimer and monomer bands for Prph2 and Rom1 are detected in retinal extracts from WT, *Prph2*$^{+/-}$, *Prph2*$^{C/+}$, and *Phrph2*$^{C/C}$ mice. Although both bands are present in *Prph2*$^{C/C}$ retinal extracts, the majority of C213Y Prph2 is present as a monomer. This suggests that the mutant protein has only limited ability to form covalently bound complexes. Although overall Rom1 levels are reduced in the *Prph2*$^{C/C}$, Rom1 appeared equally in monomer and dimer forms, suggesting that C213Y Prph2 did not alter the ability of Rom1 to form disulfide-linked homomeric complexes.

Both IP and nonreducing immunoblot analyses suggest that C213Y Prph2 has impaired oligomerization. To assess the nature of complexes formed by the C213Y Prph2, nonreducing sucrose gradient velocity sedimentation[13,16,26] was performed. In the WT retina, Prph2 presents as tetramers (fractions 6–8), intermediate complexes (fractions 4–5), and higher order oligomers (fractions 1–3), while Rom1 is detected only in tetramers and intermediate oligomers. We did not observe a significant difference in Prph2 complex formation between the WT and *Prph2*$^{+/-}$ retinas (Figure 2C). However, virtually no higher

order or intermediate complexes were observed in the *Prph2*$^{C/C}$. Instead, C213Y Prph2 was present only in tetrameric and lighter fractions. In the *Prph2*$^{C/+}$, there was a reduction in Prph2 in fractions 3–4 with an increase in fraction 7 and a slight increase in fraction 1. These findings show that C213Y Prph2 alone cannot form higher order and intermediate complexes and may also impair the ability of WT Prph2 to assemble into a normal complement of larger complexes.

The pattern of Rom1 complexes in the *Prph2*$^{+/-}$ and *Prph2*$^{C/+}$ are similar, with an overall broadening of Rom1 distribution. This results in increased Rom1 in both the lighter fractions (7–9) as well as the heavier fractions (1–3, arrows Figure 2D) compared to WT. The increased presence of Rom1 in heavier fractions (fractions 1–3) in the *Prph2*$^{+/-}$ and *Prph2*$^{C/+}$, though representing a very small fraction of total Rom1, is likely due to the reduction in the amount of WT Prph2 available to form large complexes and suggests Rom1 can compensate in a small way for reduced Prph2. In *Prph2*$^{C/C}$ retinas, Rom1 was substantially right-shifted, appearing almost exclusively in tetramer and lighter fractions (Figure 2D). This finding, combined with the lack of interaction between Rom1 and C213Y Prph2, supports the hypothesis that covalently linked intermediate sized Rom1 complexes (ie, fractions 4–5) are typically Prph2/Rom1 heteromers rather than homomeric Rom1 complexes.

3.3 | Expression of C213Y Prph2 leads to early onset decline in scotopic and photopic light evoked responses

Since total Prph2 in *Prph2*$^{C/+}$ was similar to *Prph2*$^{+/-}$, we predicted that the phenotype in the *Prph2*$^{C/+}$ mouse would be rod-dominant RP and not a cone-rod or butterfly pattern dystrophy as observed in patients.[23] To evaluate rod function, full-field scotopic ERG was performed (Figure 3A shows representative scotopic ERG traces from P30 mice). A significant (~60%) reduction in maximum scotopic a-wave amplitude was observed in *Prph2*$^{C/+}$ when compared to WT at P30 (Figure 3B). A similar reduction was observed in maximum scotopic b-wave amplitudes (Figure 3B, right panel) and persisted at P180 and P365 (Figure 3C–D). This decline in scotopic function in the *Prph2*$^{C/+}$ was more severe than that in the *Prph2*$^{+/-}$. We detected little to no scotopic response in *Prph2*$^{C/C}$ mice at early time points (similar to the *Prph2*$^{-/-}$, Figure 3B), so homozygous animals were excluded from later time point evaluations.

We next evaluated the effect of C213Y Prph2 on cones by performing full-field photopic ERG (Figure 4A shows representative traces) on light adapted animals at P30, P180, and P365. Cone function in the *Prph2*$^{C/+}$ was significantly reduced at P30 (Figure 4B) when compared to WT and *Prph2*$^{+/-}$ and was further reduced at P180 and P365 (Figure 4C–D). Surprisingly, though very low compared to WT, average photopic b-wave in the *Prph2*$^{C/C}$ was significantly better than age-matched *Prph2*$^{-/-}$ (Figure 4A,B). These findings clearly demonstrate that the C213Y mutation causes dominant functional defects in both rods and cones rather than a rod-dominant RP phenotype.

3.4 | C213Y Prph2 knockin exhibited funduscopic abnormalities consistent with patient phenotypes

One of the foremost features of butterfly pattern dystrophy associated with C213Y Prph2 is the characteristic funduscopic changes that occur due to defects in the choroid and RPE, including accumulation of lipofuscin in the RPE.[23] At P30, no fundus abnormalities in C213Y mice or other genotypes were detected (Figure 5A). However, by P180, the *Prph2*$^{C/+}$ fundus exhibited a pronounced retinal flecking phenotype we have previously seen in pattern dystrophy models (black arrows highlight examples of flecking in Figure 5B) which are not seen in age-matched WT or *Prph2*$^{+/-}$. Similarly, yellow flecking was more pronounced at P180 in the *Prph2*$^{C/C}$ compared to age-matched *Prph2*$^{-/-}$. Retinal vasculature as assessed by fluorescein angiography was largely normal at P180 in all genotypes (Figure 5B, lower panels). The yellow flecking in the *Prph2*$^{C/+}$ persisted at P365, while the flecking in *Prph2*$^{-/-}$ and *Prph2*$^{C/C}$ was masked by large splotchy areas (asterisks Figure 5C) which align with leaky vasculature observed on fluorescein angiograms. We have previously observed these splotches[18] in other knockin models, and hypothesize that they arise as a result of ongoing retinal degeneration, which is quite severe in the *Prph2*$^{-/-}$ by P365. Though the origin of the flecking in the *Prph2*$^{C/+}$ is not yet known, these data suggest that the C213Y animal model exhibits clinical signs of C213Y-associated disease, likely due to the presence of the mutant protein, rather than the reduction in overall Prph2 levels alone.

3.5 | C213Y Prph2 initiates disc formation in the presence of WT Prph2

To evaluate whether observed functional defects were associated with retinal degeneration or defects in OS structure, histologic analyses were performed at the light (Figure 6A) and electron microscopic (Figure 6B) levels. At P30, the *Prph2*$^{C/C}$ had obvious degeneration/thinning of the outer nuclear layer and OSs that were very hard to detect (Figure 6A). Evaluation at higher magnification shows that, while *Prph2*$^{-/-}$ produced no observable OSs or OS-like structures, the *Prph2*$^{C/C}$ retinas produced highly disorganized membranous, disc-like structures (Figure 6B, arrows), suggesting that OS formation was initiated but could not be completed by the C213Y mutant protein alone.

Overall retinal appearance was similar in the *Prph2*$^{C/+}$ and *Prph2*$^{+/-}$ retinas (Figure 6A), however, *Prph2*$^{C/+}$ had a modest increase in ONL degeneration compared to *Prph2*$^{+/-}$ or WT (Figure 6C). On electron micrographs, OS alignment and disc stacking were improved at P30 in *Prph2*$^{C/+}$ in comparison to *Prph2*$^{+/-}$ (Figure 6B), and this structural improvement persisted at P180 (Figure 6F). However, the observed OS structures in *Prph2*$^{C/+}$ were still completely irregular compared to the WT, and improved disc structure did not result in improved OS length (Figure 6C, right panels) or improved rhodopsin levels (Figure 6D,E). We observed decreased rhodopsin levels in the *Prph2*$^{+/-}$, *Prph2*$^{C/+}$, *Prph2*$^{-/-}$, and *Prph2*$^{C/C}$. This decrease is likely due to a combination of photoreceptor degeneration, OS shortening, and reductions in rhodopsin protein independent of structural concerns. To help tease out these differences, we plotted mean rhodopsin levels (Figure 6D) as a ratio to the ONL and OS thickness (Figure 6E). Decreased ONL thickness (ie, photoreceptor degeneration) does not account for the decreased rhodopsin levels in the *Prph2*$^{+/-}$ and *Prph2*$^{C/+}$ (Figure 6E, top). In contrast, plotting rhodopsin levels as a ratio to OS length demonstrates that the reduction in rhodopsin seen in the *Prph2*$^{+/-}$ is accounted for by reduced OS length (Figure

6E, bottom). After normalizing to OS length, rhodopsin levels in the *Prph2*$^{C/+}$ remain slightly lower than in the *Prph2*$^{+/-}$ and WT, though the difference is not statistically significant.

3.6 | C213Y Prph2 exhibits OS trafficking defects

The OS trafficking signal of Prph2 is present in its C-terminus.[31,32] However, mutations in the D2 loop of Prph2 can also lead to accumulation of mutant Prph2 in the inner segment of cones.[29] To evaluate whether the mutant C213Y Prph2 properly localized to the OS, we performed immunofluorescence labeling on P30 retinal sections (Figure 7A–H). Co-labeling of Prph2 with Rom1, rhodopsin, M-opsin, and S-opsin shows proper OS labeling of all target proteins in the WT and *Prph2*$^{+/-}$ retinas (Figure 7A,B,E,F). In *Prph2*$^{C/+}$ we observed mislocalization of Prph2 (green) to the inner segment and perinuclear region in addition to labeling the OS (Figure 7C,G, arrows). This phenotype is more pronounced in the *Prph2*$^{C/C}$ retina where Prph2 was primarily located in the ONL and inner segments (white arrows in Figure 7D,H), suggesting that mutant Prph2 protein cannot traffic to the OS on its own. Most Rom1 successfully transported to the OS in the *Prph2*$^{C/+}$ and *Prph2*$^{C/C}$ (red arrows, Figure 7D,H) although a small amount appears in the IS with mislocalized Prph2. Although Prph2 and Rom1 normally co-localize in the OS, this was not observed in the *Prph2*$^{C/C}$; Rom1 is found in the OS layer without appreciable Prph2 (red arrows, Figure 7H, right). This strikingly abnormal distribution of Prph2/Rom1 in the *Prph2*$^{C/C}$ is consistent with our finding that Rom1 did not interact with C213Y Prph2. Rhodopsin and S-Opsin were also mislocalized in the *Prph2*$^{C/C}$ (Figure 7D,H, yellow arrows). To further assess localization of Prph2 in the malformed *Prph2*$^{C/+}$ and *Prph2*$^{C/C}$ OSs, we conducted immunogold labeling (Figure 7I). Prph2 and Rom1 are present, albeit drastically reduced, in the OSs of both *Prph2*$^{C/+}$ and *Prph2*$^{C/C}$ (see arrowheads and insets in Figure 7I). Importantly, Prph2 and Rom1 correctly localize to the disc rim region in the *Prph2*$^{C/+}$, though not in the *Prph2*$^{C/C}$ which lacks properly formed rims. The tiny abnormal OS structures in the *Prph2*$^{C/C}$ also labeled with rhodopsin and cone opsins, suggesting that they are nascent OSs in spite of their inability to mediate substantial ERG function.

Having observed accumulation of mutant proteins in the outer nuclear layer and inner segments of both *Prph2*$^{C/+}$ and *Prph2*$^{C/C}$ retinas, we asked whether this led to endoplasmic reticulum (ER) stress or autophagy, often a byproduct of accumulation of misfolded proteins. Endoplasmic reticulum stress can initiate autophagy and related programed cell death mechanisms,[33] and this pathway has been previously evaluated for its potential impact on retinal degeneration in the presence of protein aggregates and/or malformations in the photoreceptor disc.[18,34] We tested for the cleavage and activation of XBP1 mRNA (Figure 8A), the expression of genes central to the ER stress pathway (Figure 8B), and proteins involved in stress-induced autophagy flux (Figure 8C). We observed no activation of the XBP1 mRNA, nor any change in the expression of factors associated with ER stress (ATF4, BiP) or apoptosis (CHOP) in any genotype (thapsigargin treatment was used as a positive control). Similarly, we observed no change in markers of autophagy such as the LC3B-II/I ratio and Beclin 1 protein expression. These results indicate that the observed retinal degeneration in *Prph2*$^{C/+}$ and *Prph2*$^{C/C}$ mice is not the result of cell death mechanisms

related to ER stress or autophagy, and that the observed accumulation of Prph2 in the inner segments and perinuclear area is not inducing detectable ER stress.

3.7 | Gene supplementation does not rescue the pathological phenotype associated with C213Y Prph2

Because the level of expression of Prph2 protein is critical to OS structure and function, gene supplementation has often been an attractive therapeutic goal. The significantly reduced Prph2 protein levels in the *Prph2*$^{C/+}$ suggested this model might be amenable to such an approach. To test this hypothesis, we utilized our transgenic mouse line that overexpresses WT peripherin (NMP).[25] One allele of this photoreceptor-specific transgene results in expression of ~30% of the WT Prph2 levels,[25] and can rescue haploinsufficiency in the *Prph2*$^{+/-}$, without causing overexpression-associated toxicity when expressed on the WT background. After backcrossing the NMP mouse with the *Prph2*$^{C/C}$ to get NMP/*Prph2*$^{C/+}$, we evaluated Prph2, Rom1, and rhodopsin levels by immunoblot (Figure 9A). In the NMP/*Prph2*$^{C/+}$ retina, Prph2, Rom1, and rhodopsin were rescued to WT levels and were significantly higher than their levels in *Prph2*$^{C/+}$ and *Prph2*$^{+/-}$. Immunofluorescent evaluation of NMP/*Prph2*$^{C/+}$ retinas also showed proper OS localization of Prph2, rhodopsin, and S-opsin without the pronounced Prph2 mislocalization to the inner segment and perinuclear regions seen in the *Prph2*$^{C/+}$ (Figure 9B). Similarly, OS organization was significantly improved in the *NMP/Prph2*$^{C/+}$ compared to the *Prph2*$^{C/+}$ (Figure 9C).

However, in spite of these improvements in protein levels, protein trafficking, and disc structure, photoreceptor function was not rescued in NMP/*Prph2*$^{C/+}$ compared to age-matched *Prph2*$^{C/+}$ and *Prph2*$^{+/-}$ mice (Figure 10A, purple lines). Scotopic ERG responses from *NMP*$^{+/-}$/*Prph2*$^{C/+}$ at P30 were slightly higher than *Prph2*$^{C/+}$ but were significantly lower than the WT and were comparable to *Prph2*$^{+/-}$. Cone function was likewise not improved in the NMP/*Prph2*$^{C/+}$ at P30. However, age-related loss-of-function was slower in the NMP/*Prph2*$^{C/+}$ than in WT or *Prph2*$^{C/+}$ with the result that at P365 rod function in NMP/*Prph2*$^{C/+}$ was 80% of WT and cone function was comparable to WT (Figure 10A). Fundus phenotypes in the NMP/*Prph2*$^{C/+}$ eyes were variable; Figure 10B shows three representative eyes. In some cases, retinal flecking was reduced compared to *Prph2*$^{C/+}$, while in others no change was detected. Despite the improved protein expression levels and OS structures, the failure of Prph2 overexpression to rescue the functional phenotype at young ages suggests that combination of gene supplementation and knockdown is the proper strategy to efficiently treat patients with C213Y Prph2 mutation.

4 | DISCUSSION

D2 loop disulfide bonds are essential for proper folding, stability, and subunit assembly for all tetraspanin proteins including Prph2.[35,36] The tetraspanin D2 loop has been extensively characterized and contains both a highly conserved region and a hypervariable region.[35,37] The highly conserved region is formed by two alpha helices at the N-terminal of the D2 loop and a third alpha helix at the C-terminal, while the highly variable region is found between the second and third helices[36] (Figure 11). The six highly conserved D2 loop cysteines involved in intramolecular disulfide bonding are essential for maintaining the secondary and

tertiary structure of the D2 loop.[13,38] These six cysteines form three intramolecular disulfide linkages, Cys165-Cys250, Cys214-Cys222, and Cys166-Cys213, predicted based on alignment with other crystallized tetraspanins.[39] Of these six cysteines, mutations in five have secondary macular involvement).[17,40–42] In contrast, are pathogenic. Mutations in both Cys165 and its pair mutations in Cys213 are associated with pattern and macuCys250[40,41] as well as Cys214 and its pair Cys222 are as- lar dystrophy,[23,43] while no pathogenic mutations have sociated with RP (though Cys250-associated RP can also been identified in Cys166.

In vitro experiments have suggested that mutations in any of these six cysteines lead to protein aggregation.[13] In addition, Prph2 carrying mutations at Cys166 and Cys214 do not form normal tetramers, and instead are present either as large insoluble aggregates or a distinct, abnormal species of noncovalently linked dimers.[13] Here we find that in vivo C213Y Prph2 exhibits an intermediate molecular phenotype. Like WT Prph2, C213Y retains the ability to form tetramers and does not form large insoluble aggregates, but like C214S Prph2,[8,13] it loses the ability to interact with Rom1 and is also shifted into lighter gradient fractions corresponding to noncovalently linked dimers. Our finding that in spite of having normal transcript levels, C214S Prph2 protein is undetectable in transgenic mice[8] has led to the hypothesis that interruption of the Cys214-Cys222 disulfide linkage results in protein that is sufficiently misfolded to be quickly degraded. This is quite different from C213Y protein. The fact that C213Y Prph2 can form tetramers and does not form aggregates suggests it is not as misfolded as C214S protein. The reduced levels of C213Y protein are therefore likely due to its inability to support OS formation rather than biochemical instability; that is, in the absence of elaborated OSs, Prph2 accumulates in the inner segment and ONL (where it is ultimately degraded) simply because it does not have an OS to reside in. We find precedence for this in the case of rhodopsin (as well as other Prph2 mutants such as K153del[14]), which is reduced and mislocalized in the *Prph2*$^{-/-}$[26] and *Prph2*$^{C/C}$ not because rhodopsin is unstable without Prph2 but because there are no OSs.

Yet the question remains, why should the C213Y mutation affect the Prph2 protein and lead to functional and structural phenotypes so different from C214S and the other cysteine mutations that cause RP? In the case of Cys214-Cys222 and Cys165-Cys250, mutation in either cysteine of the pair leads to the same disease phenotype, suggesting that it is removal of the disulfide bond (and consequent structural changes) rather than substitution of a different amino acid that causes the defect in those cases. It is likely that removal of the disulfide bond also underlies the C213Y phenotype. Cys166-Cys213 holds together a much smaller region of the D2 loop than Cys165-Cys250 (which stabilizes the entire hypervariable region of the D2 loop). In addition, the Cys166-Cys213 bond is directly in the middle of the region required for Prph2-Rom1 interactions (Figure 11), and thus altering the structure of that region might be predicted to affect Prph2-Rom1 bonding, while preserving the ability to form Prph2 homotetramers (which are assembled via interactions in a smaller area of the D2 loop[9]). In addition to effects due to removal of the Cys166-Cys213 intramolecular disulfide linkage, there may also be effects due to alterations in intermolecular disulfide linkages. C213Y protein does not form covalently linked higher order complexes alone, suggesting that either the freed cysteine (Cys166) is forming a new intramolecular disulfide bond with Cys150 or that the folding defects consequent to the C213Y mutation block access to

Cys150. Critically, even in the presence of WT Prph2, the C213Y protein is not capable of complexing normally; *Prph2*$^{C/+}$ retinas exhibit reductions in large-to-intermediate sized Prph2 complexes (fractions 2–4) and a slight increase in the largest complexes (in fraction 1) as well as tetramers (fraction 7). Interestingly, the increase in fraction 1 also occurs in the *Prph2*$^{+/-}$, something we have also seen previously, while the alterations in fractions 3,4, and 7 are unique to the *Prph2*$^{C/+}$. We hypothesize that this alteration in the complexes in fraction 1 may be tied to changes in OS structure that are common in the *Prph2*$^{+/-}$ and *Prph2*$^{C/+}$, while the changes in the other fractions (3, 4, and 7) are due to biochemical defects in the C213Y Prph2 protein such as its inability to bind Rom1. However, understanding the specific roles of different types of Prph2 complexes and their connection to OS structure remains an interesting unanswered question.

Due to complete degradation of the C214S protein, C214S heterozygous mice exhibit a pure loss-of-function haploinsufficiency phenotype in which rod function and structure are compromised and cone function is preserved until later in life (indistinguishable from the *Prph2*$^{+/-}$).[5,8] Here we observed similarly reduced Prph2 levels in C213Y heterozygous mice, suggesting it could also be a loss-of-function allele. However, in contrast to other haploinsufficiency mutants, the C213Y mutation causes significant defects in both rod and cone function. Some dominant negative Prph2 mutations, such as P216L,[44] lead to degradation of both mutant and WT Prph2 resulting in severe haploinsufficiency and early onset RP. This does not appear to be the case for C213Y however, which has similar Prph2 protein levels in the *Prph2*$^{C/+}$ and *Prph2*$^{+/-}$. Other Prph2 mutations, such as R172W and Y141C,[18,45,46] are clear gain-of-function mutations; both the mutant and WT Prph2 proteins are stable, yet defects in cone and/or rod structure and function occur. In the case of C213Y, reduced Prph2 levels, the presence of rod and cone targeted defects, and the inability to significantly improve functional phenotypes by the addition of extra WT Prph2 suggest that C213Y exerts both loss-of-function and gain-of-function effects in rods and cones.

While the *Prph2*$^{C/+}$ animals exhibit worse rod and cone function than their *Prph2*$^{+/-}$ counterparts, they exhibit slightly better rod structure (though not length). Previous studies found that a 50% reduction in Prph2 (*Prph2*$^{+/-}$) produces whorl-like OS structures.[5] Here, replacing the null allele with that of C213Y Prph2 (*Prph2*$^{C/+}$) results in improved rod disc organization. Since *Prph2*$^{+/-}$ and *Prph2*$^{C/+}$ have similar amounts of Prph2, this structural improvement could be a result of the increased amount of Rom1 protein in the *Prph2*$^{C/+}$. However, our rescue experiments with supplementation of WT show that having enough Prph2 and Rom1 is not sufficient for proper OS structure and function if C213Y mutant protein is still present. This may be because Prph2 is not only an important structural component of the OS, but also plays a critical role in organizing functional protein domains at the OS disc rim, thus optimizing visual signaling in response to light stimuli.[47–49] Prph2 interacts with several proteins critical to phototransduction, including the beta subunit of the rod cyclic nucleotide gated channel (CNGB1), the cytosolic isoforms of CNGB1 called GARPs,[49,50] rhodopsin,[51] and cone opsins.[52] Furthermore, the Prph2 cone-dominant macular dystrophy mutation, V268I, has been shown to specifically affect Prph2 binding to M-opsin but not S-opsin or rhodopsin,[52] supporting the idea that Prph2 may play a key role in organizing functional protein domains and that disease mutations may adversely affect these functional domains. Interestingly, we find that S-opsin but not M-opsin is mislocalized

in *Prph2*$^{C/C}$ retinas. Studies have shown that Prph2 traffics separately from rod and cone opsins.[53–55] In addition, cone opsin mislocalization often precedes cone degeneration even if the toxic signal is not an OS protein (eg, in the *Rpe65*$^{-/-}$ or *Lrat*$^{-/-}$[56,57]), suggesting the mislocalized cone opsin may be due to incipient or ongoing degeneration. Why we should observe S-opsin mislocalization without M-opsin mislocalization is not clear, especially since S- and M-cone function are similarly affected by the C213Y mutation. However, the pattern of more severe S-opsin mislocalization than M-opsin mislocalization was also observed in the *Rpe65*$^{-/-}$ mouse,[56] raising the idea that the difference has more to do with native properties of murine cones than anything specific about Prph2 or the C213Y mutation. Certainly exploration of the interplay and functional role of Prph2/opsin trafficking and Prph2/opsin complex assembly in rods vs. cones is an exciting area for future study.

While mice lack a macula, the C213Y knockin mice do exhibit some of the clinical phenotypes such as fundus speckling that characterize Prph2-associated pattern dystrophy. Prph2-associated macular dystrophy and pattern dystrophy are often accompanied by deleterious effects on tissues outside the photoreceptors including the choroid and RPE,[1] and yellowish flecking on the fundus has been recognized to arise from defects in the RPE, accumulation of lipofuscin in the RPE, and defects in the choroidal vasculature.[58] The clear-cut origin of the flecking we observe in the C213Y animals is not known and long-term studies evaluating this will be critical next steps.

Haploinsufficiency associated with loss of function alleles (as in the case of the *Prph2*$^{+/-}$ or the C214S Prph2 models), is in principle the ideal situation for treatment by gene supplementation. For example, when using the NMP transgene to supplement WT Prph2 (the same approach used here) in the C214S Prph2 or *Prph2*$^{+/-}$ model, we achieved structural and functional rescue.[25,59] However, though both viral and non-viral genetic interventions have been attempted for the treatment of *Prph2*$^{-/-}$[6,60] and *Prph2*$^{+/-}$,[7] to date no study has reported significant functional and structural rescue because exogenously delivered gene therapies have been unable to generate sufficient Prph2 expression levels.[25] The situation is even more complex if mutations have dominant negative or gain-of-function defects. Because defects in the C213Y model appeared to be a blend of haploinsufficiency/loss-of-function effects and gain-of-function effects, we here tested whether gene supplementation for C213Y Prph2 associated phenotype would be an effective strategy. Although we found supplementation with WT Prph2 in the *Prph2*$^{C/+}$ significantly increased Prph2, Rom1, and rhodopsin levels to that of WT and significantly improved OS structure, it did not appreciably rescue the functional defects in rods or cones. This finding is quite striking and highlights the idea that both rods and cones are affected by gain-of-function effects of the C213Y Prph2 mutation. Our results emphasize the fact that gene supplementation alone for *Prph2*$^{C/+}$ is unlikely to be a clinically viable treatment strategy and future therapeutic approaches will need to target the mutant allele with concomitant gene supplementation.

ACKNOWLEDGMENTS

The authors would like to thank Ms. Barb Nagel for technical assistance. We would also like to thank Dr. Robert Molday (University of British Columbia), Dr. Cheryl Craft (University of Southern California), Dr. Andrew Goldberg (Oakland University), and Dr. Steve Fliesler (University at Buffalo, SUNY) for providing antibodies as indicated in the text. Funding for this project was provided by award EY010609 from the National Eye Institute to MIN and MRA.

Funding information

NEI/NIH, Grant/Award Number: EY010609

Abbreviations:

ATF4	activating transcription factor 4
BiP	binding immunoglobulin protein (aka GRP-78)
CHOP	C/EBP homologous binding protein
Co-IP	co-immunoprecipitation
DTT	dithiothreitol
ER	endoplasmic reticulum
ERG	electroretinography
Hprt	hypoxanthine phosphoribosyltransferase
IRBP	interphotoreceptor retinoid binding protein
LC3B	microtubule-associated protein light chain 3 variant B
NMP	normal mouse Prph2
NRL	neural retina leucine zipper
ONL	outer nuclear layer
OS	photoreceptor outer segment
P	postnatal day
PNGase	peptide-N-glycosidase
PRPH2	prph2, peripherin/rds
Rom1	rod outer segment membrane protein 1
RP	retinitis pigmentosa
SDS-PAGE	SDS-polyacrylamide gel electrophoresis
TEM	transmission electron microscopy
XBP1	X-box binding protein

WT wild type

REFERENCES

1. Boon CJ, den Hollander AI, Hoyng CB, Cremers FP, Klevering BJ, Keunen JE. The spectrum of retinal dystrophies caused by mutations in the peripherin/RDS gene. Prog Retin Eye Res. 2008;27:213–235. [PubMed: 18328765]
2. Conley SM, Stuck MW, Watson JN, Naash MI. Rom1 converts Y141C-Prph2-associated pattern dystrophy to retinitis pigmentosa. Hum Mol Genet. 2017;26:509–518. [PubMed: 28053051]
3. Shankar SP, Hughbanks-Wheaton DK, Birch DG, et al. Autosomal dominant retinal dystrophies caused by a founder splice site mutation, c.828+3A>T, in PRPH2 and protein haplotypes in trans as modifiers. Invest Ophthalmol Vis Sci. 2016;57:349–359. [PubMed: 26842753]
4. Poloschek CM, Bach M, Lagreze WA, et al. ABCA4 and ROM1: implications for modification of the PRPH2-associated macular dystrophy phenotype. Invest Ophthalmol Vis Sci. 2010;51: 4253–4265. [PubMed: 20335603]
5. Cheng T, Peachey NS, Li S, Goto Y, Cao Y, Naash MI. The effect of peripherin/rds haploinsufficiency on rod and cone photoreceptors. J Neurosci. 1997;17:8118–8128. [PubMed: 9334387]
6. Ali RR, Sarra GM, Stephens C, et al. Restoration of photoreceptor ultrastructure and function in retinal degeneration slow mice by gene therapy. Nat Genet. 2000;25:306–310. [PubMed: 10888879]
7. Cai X, Nash Z, Conley SM, Fliesler SJ, Cooper MJ, Naash MI. A partial structural and functional rescue of a retinitis pigmentosa model with compacted DNA nanoparticles. PLoS One. 2009;4:e5290. [PubMed: 19390689]
8. Stricker HM, Ding XQ, Quiambao A, Fliesler SJ, Naash MI. The Cys214–>Ser mutation in peripherin/rds causes a loss-of-function phenotype in transgenic mice. Biochem J. 2005;388:605–613. [PubMed: 15656787]
9. Ding XQ, Stricker HM, Naash MI. Role of the second intradiscal loop of peripherin/rds in homo and hetero associations. Biochemistry. 2005;44:4897–4904. [PubMed: 15779916]
10. Kedzierski W, Weng J, Travis GH. Analysis of the rds/peripherin. rom1 complex in transgenic photoreceptors that express a chimeric protein. J Biol Chem. 1999;274:29181–29187. [PubMed: 10506174]
11. Jansen HG, Sanyal S. Development and degeneration of retina in rds mutant mice: electron microscopy. J Comp Neurol. 1984;224:71–84. [PubMed: 6715580]
12. Loewen CJ, Molday RS. Disulfide-mediated oligomerization of Peripherin/Rds and Rom-1 in photoreceptor disk membranes. Implications for photoreceptor outer segment morphogenesis and degeneration. J Biol Chem. 2000;275:5370–5378. [PubMed: 10681511]
13. Goldberg AF, Loewen CJ, Molday RS. Cysteine residues of photoreceptor peripherin/rds: role in subunit assembly and autosomal dominant retinitis pigmentosa. Biochemistry. 1998;37:680–685. [PubMed: 9425091]
14. Chakraborty D, Conley SM, Zulliger R, Naash MI. The K153Del PRPH2 mutation differentially impacts photoreceptor structure and function. Hum Mol Genet. 2016;25:3500–3514. [PubMed: 27365499]
15. Zulliger R, Conley SM, Mwoyosvi ML, Al-Ubaidi MR, Naash MI. Oligomerization of Prph2 and Rom1 is essential for photoreceptor outer segment formation. Hum Mol Genet. 2018;27: 3507–3518. [PubMed: 29961824]
16. Chakraborty D, Ding XQ, Conley SM, Fliesler SJ, Naash MI. Differential requirements for retinal degeneration slow intermolecular disulfide-linked oligomerization in rods versus cones. Hum Mol Genet. 2009;18:797–808. [PubMed: 19050038]
17. Saga M, Mashima Y, Akeo K, Oguchi Y, Kudoh J, Shimizu N. A novel Cys-214-Ser mutation in the peripherin/RDS gene in a Japanese family with autosomal dominant retinitis pigmentosa. Hum Genet. 1993;92:519–521. [PubMed: 8244346]
18. Stuck MW, Conley SM, Naash MI. The Y141C knockin mutation in RDS leads to complex phenotypes in the mouse. Hum Mol Genet. 2014;23:6260–6274. [PubMed: 25001182]

19. Vaclavik V, Tran HV, Gaillard MC, Schorderet DF, Munier FL. Pattern dystrophy with high intrafamilial variability associated with Y141C mutation in the peripherin/RDS gene and successful treatment of subfoveal CNV related to multifocal pattern type with anti-VEGF (ranibizumab) intravitreal injections. Retina. 2012;32:1942–1949. [PubMed: 22466463]
20. Weleber RG, Carr RE, Murphey WH, Sheffield VC, Stone EM. Phenotypic variation including retinitis pigmentosa, pattern dystrophy, and fundus flavimaculatus in a single family with a deletion of codon 153 or 154 of the peripherin/RDS gene. Arch Ophthalmol. 1993;111:1531–1542. [PubMed: 8240110]
21. Fossarello M, Bertini C, Galantuomo MS, Cao A, Serra A, Pirastu M. Deletion in the peripherin/RDS gene in two unrelated Sardinian families with autosomal dominant butterfly-shaped macular dystrophy. Arch Ophthalmol. 1996;114:448–456. [PubMed: 8602784]
22. Nichols BE, Sheffield VC, Vandenburgh K, Drack AV, Kimura AE, Stone EM. Butterfly-shaped pigment dystrophy of the fovea caused by a point mutation in codon 167 of the RDS gene. Nat Genet. 1993;3:202–207. [PubMed: 8485574]
23. Zhang K, Garibaldi DC, Li Y, Green WR, Zack DJ. Butterfly-shaped pattern dystrophy: a genetic, clinical, and histopathological report. Arch Ophthalmol. 2002;120:485–490. [PubMed: 11934323]
24. Stuck MW, Conley SM, Naash MI. Retinal degeneration slow (RDS) glycosylation plays a role in cone function and in the regulation of RDS.ROM-1 protein complex formation. J Biol Chem. 2015;290:27901–27913. [PubMed: 26420485]
25. Nour M, Ding XQ, Stricker H, Fliesler SJ, Naash MI. Modulating expression of peripherin/rds in transgenic mice: critical levels and the effect of overexpression. Invest Ophthalmol Vis Sci. 2004;45:2514–2521. [PubMed: 15277471]
26. Chakraborty D, Ding XQ, Fliesler SJ, Naash MI. Outer segment oligomerization of Rds: evidence from mouse models and subcellular fractionation. Biochemistry. 2008;47:1144–1156. [PubMed: 18171083]
27. Farjo R, Skaggs JS, Nagel BA, et al. Retention of function without normal disc morphogenesis occurs in cone but not rod photoreceptors. J Cell Biol. 2006;173:59–68. [PubMed: 16585269]
28. Koirala A, Makkia RS, Conley SM, Cooper MJ, Naash MI. S/MAR-containing DNA nanoparticles promote persistent RPE gene expression and improvement in RPE65-associated LCA. Hum Mol Genet. 2013;22:1632–1642. [PubMed: 23335596]
29. Chakraborty D, Conley SM, Stuck MW, Naash MI. Differences in RDS trafficking, assembly and function in cones versus rods: insights from studies of C150S-RDS. Hum Mol Genet. 2010;19:4799–4812. [PubMed: 20858597]
30. Goldberg AF, Molday RS. Defective subunit assembly underlies a digenic form of retinitis pigmentosa linked to mutations in peripherin/rds and rom-1. Proc Natl Acad Sci USA. 1996;93:13726–13730. [PubMed: 8943002]
31. Tam BM, Moritz OL, Papermaster DS. The C terminus of peripherin/rds participates in rod outer segment targeting and alignment of disk incisures. Mol Biol Cell. 2004;15:2027–2037. [PubMed: 14767063]
32. Salinas RY, Baker SA, Gospe SM 3rd, Arshavsky VY. A single valine residue plays an essential role in peripherin/rds targeting to photoreceptor outer segments. PLoS One. 2013;8:e54292. [PubMed: 23342122]
33. Zhang SX, Sanders E, Fliesler SJ, Wang JJ. Endoplasmic reticulum stress and the unfolded protein responses in retinal degeneration. Exp Eye Res. 2014;125:30–40. [PubMed: 24792589]
34. Bhattacharya S, Yin J, Winborn CS, Zhang Q, Yue J, Chaum E. Prominin-1 is a novel regulator of autophagy in the human retinal pigment epithelium. Invest Ophthalmol Vis Sci. 2017;58:2366–2387. [PubMed: 28437526]
35. Stuck MW, Conley SM, Naash MI. PRPH2/RDS and ROM-1: historical context, current views and future considerations. Prog Retin Eye Res. 2016;52:47–63. [PubMed: 26773759]
36. Conley SM, Stuck MW, Naash MI. Structural and functional relationships between photoreceptor tetraspanins and other superfamily members. Cell Mol Life Sci. 2012;69:1035–1047. [PubMed: 21655915]
37. Conley SM, Naash MI. Gene therapy for PRPH2-associated ocular disease: challenges and prospects. Cold Spring Harb Perspect Med. 2014;4:a017376. [PubMed: 25167981]

38. Chakraborty D, Rodgers KK, Conley SM, Naash MI. Structural characterization of the second intra-discal loop of the photoreceptor tetraspanin RDS. FEBS J. 2013;280:127–138. [PubMed: 23121719]
39. Seigneuret M, Delaguillaumie A, Lagaudriere-Gesbert C, Conjeaud H. Structure of the tetraspanin main extracellular domain. A partially conserved fold with a structurally variable domain insertion. J Biol Chem. 2001;276:40055–40064. [PubMed: 11483611]
40. Souied EH, Rozet JM, Gerber S, et al. Two novel missense mutations in the peripherin/RDS gene in two unrelated French patients with autosomal dominant retinitis pigmentosa. Eur J Ophthalmol. 1998;8:98–101. [PubMed: 9673478]
41. Katagiri S, Hayashi T, Mizobuchi K, Yoshitake K, Iwata T, Nakano T. Autosomal dominant retinitis pigmentosa with macular involvement associated with a disease haplotype that included a novel PRPH2 variant (p.Cys250Gly). Ophthalmic Genet. 2018;39:357–365. [PubMed: 29630435]
42. Manes G, Guillaumie T, Vos WL, et al. High prevalence of PRPH2 in autosomal dominant retinitis pigmentosa in france and characterization of biochemical and clinical features. Am J Ophthalmol. 2015;159:302–314. [PubMed: 25447119]
43. Villaverde C, Trujillo-Tiebas MJ, Gallego-Merlo J, et al. Novel human pathological mutations. Gene symbol: RDS. Disease: macular dystrophy. Hum Genet. 2007;122:555.
44. Kedzierski W, Lloyd M, Birch DG, Bok D, Travis GH. Generation and analysis of transgenic mice expressing P216L-substituted rds/peripherin in rod photoreceptors. Invest Ophthalmol Vis Sci. 1997;38:498–509. [PubMed: 9040483]
45. Ding XQ, Nour M, Ritter LM, Goldberg AF, Fliesler SJ, Naash MI. The R172W mutation in peripherin/rds causes a cone-rod dystrophy in transgenic mice. Hum Mol Genet. 2004;13: 2075–2087. [PubMed: 15254014]
46. Conley SM, Stuck MW, Burnett JL, et al. Insights into the mechanisms of macular degeneration associated with the R172W mutation in RDS. Hum Mol Genet. 2014;23:3102–3114. [PubMed: 24463884]
47. Korschen HG, Beyermann M, Muller F, et al. Interaction of glutamic-acid-rich proteins with the cGMP signalling pathway in rod photoreceptors. Nature. 1999;400:761–766. [PubMed: 10466724]
48. Pentia DC, Hosier S, Cote RH. The glutamic acid-rich protein-2 (GARP2) is a high affinity rod photoreceptor phosphodiesterase (PDE6)-binding protein that modulates its catalytic properties. J Biol Chem. 2006;281:5500–5505. [PubMed: 16407240]
49. Poetsch A, Molday LL, Molday RS. The cGMP-gated channel and related glutamic acid-rich proteins interact with peripherin-2 at the rim region of rod photoreceptor disc membranes. J Biol Chem. 2001;276:48009–48016. [PubMed: 11641407]
50. Ritter LM, Khattree N, Tam B, Moritz OL, Schmitz F, Goldberg AF. In situ visualization of protein interactions in sensory neurons: glutamic acid-rich proteins (GARPs) play differential roles for photoreceptor outer segment scaffolding. J Neurosci. 2011;31:11231–11243. [PubMed: 21813684]
51. Becirovic E, Nguyen ON, Paparizos C, et al. Peripherin-2 couples rhodopsin to the CNG channel in outer segments of rod photoreceptors. Hum Mol Genet. 2014;23:5989–5997. [PubMed: 24963162]
52. Nguyen ON, Bohm S, Giessl A, et al. Peripherin-2 differentially interacts with cone opsins in outer segments of cone photoreceptors. Hum Mol Genet. 2016;25:2367–2377. [PubMed: 27033727]
53. Fariss RN, Molday RS, Fisher SK, Matsumoto B. Evidence from normal and degenerating photoreceptors that two outer segment integral membrane proteins have separate transport pathways. J Comp Neurol. 1997;387:148–156. [PubMed: 9331178]
54. Abd-El-Barr MM, Sykoudis K, Andrabi S, et al. Impaired photoreceptor protein transport and synaptic transmission in a mouse model of Bardet-Biedl syndrome. Vision Res. 2007;47: 3394–3407. [PubMed: 18022666]
55. Avasthi P, Watt CB, Williams DS, et al. Trafficking of membrane proteins to cone but not rod outer segments is dependent on heterotrimeric kinesin-II. J Neurosci. 2009;29:14287–14298. [PubMed: 19906976]
56. Rohrer B, Lohr HR, Humphries P, Redmond TM, Seeliger MW, Crouch RK. Cone opsin mislocalization in Rpe65−/− mice: a defect that can be corrected by 11-cis retinal. Invest Ophthalmol Vis Sci. 2005;46:3876–3882. [PubMed: 16186377]

57. Zhang T, Enemchukwu NO, Jones A, et al. Genetic deletion of S-opsin prevents rapid cone degeneration in a mouse model of Leber congenital amaurosis. Hum Mol Genet. 2015;24:1755–1763. [PubMed: 25416279]

58. Francis PJ, Schultz DW, Gregory AM, et al. Genetic and phenotypic heterogeneity in pattern dystrophy. Br J Ophthalmol. 2005;89:1115–1119. [PubMed: 16113362]

59. Nour M, Fliesler SJ, Naash MI. Genetic supplementation of RDS alleviates a loss-of-function phenotype in C214S model of retinitis pigmentosa. Adv Exp Med Biol. 2008;613:129–138. [PubMed: 18188937]

60. Sarra GM, Stephens C, de Alwis M, et al. Gene replacement therapy in the retinal degeneration slow (rds) mouse: the effect on retinal degeneration following partial transduction of the retina. Hum Mol Genet. 2001;10:2353–2361. [PubMed: 11689482]

61. Conley SM, Stuck MW, Burnett JL, et al. Insights into the mechanisms of macular degeneration associated with the R172W mutation in RDS. Hum Mol Genet. 2014;23:3102–3114. [PubMed: 24463884]

62. Stuck MW, Conley SM, Naash MI. The Y141C knockin mutation in RDS leads to complex phenotypes in the mouse. Hum Mol Genet. 2014;23:6260–6274. [PubMed: 25001182]

63. Chakraborty D, Conley SM, Al-Ubaidi MR, Naash MI. Initiation of rod outer segment disc formation requires RDS. PLoS One. 2014;9:e98939. [PubMed: 24897172]

64. MacKenzie D, Arendt A, Hargrave P, McDowell JH, Molday RS. Localization of binding sites for carboxyl terminal specific anti-rhodopsin monoclonal antibodies using synthetic peptides. Biochemistry. 1984;23:6544–6549. [PubMed: 6529569]

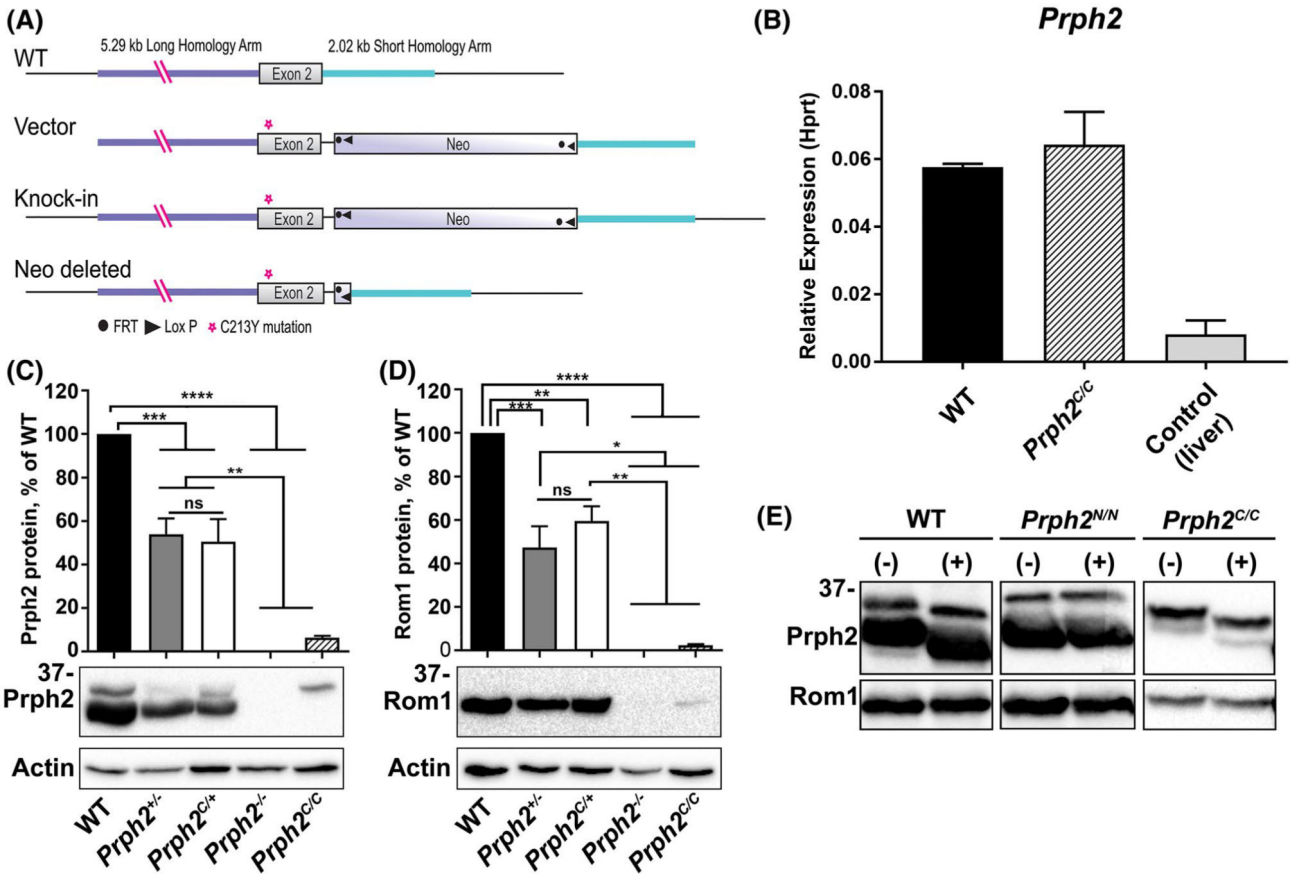

FIGURE 1.

C213Y Prph2 is expressed at very low levels. A, The C213Y mutation was introduced into exon 2 of the *Prph2* gene in order to drive properly regulated expression of the C213Y Prph2 allele. B, qRT-PCR was performed on P30 retinal cDNAs from WT and $Prph2^{C/C}$ mice using primers that recognize both WT and C213Y *Prph2* transcripts. Results were compared to cDNA isolated from liver as control. C-D, Levels of Prph2 (C) and Rom1 (D) proteins from retinal extracts of the indicated genotypes were analyzed. Band intensities were normalized to their actin levels and plotted as percent of the WT in bar graphs. E, Immunoblot of untreated and PNGase treated retinal extracts from WT, $Prph2^{N/N}$, and $Prph2^{C/C}$ probed for Prph2 and Rom1. $Prph2^{N/N}$ is a knockin model for the non-glycosylated form of Prph2 and is used as a control. Each experiment contains N = 4–8 independent retinas per genotype. Data are plotted as mean ± SEM. * $P < .05$, ** $P < .01$, *** $P < .001$, and **** $P < .0001$ by one-way ANOVA with Tukey's post-hoc comparison

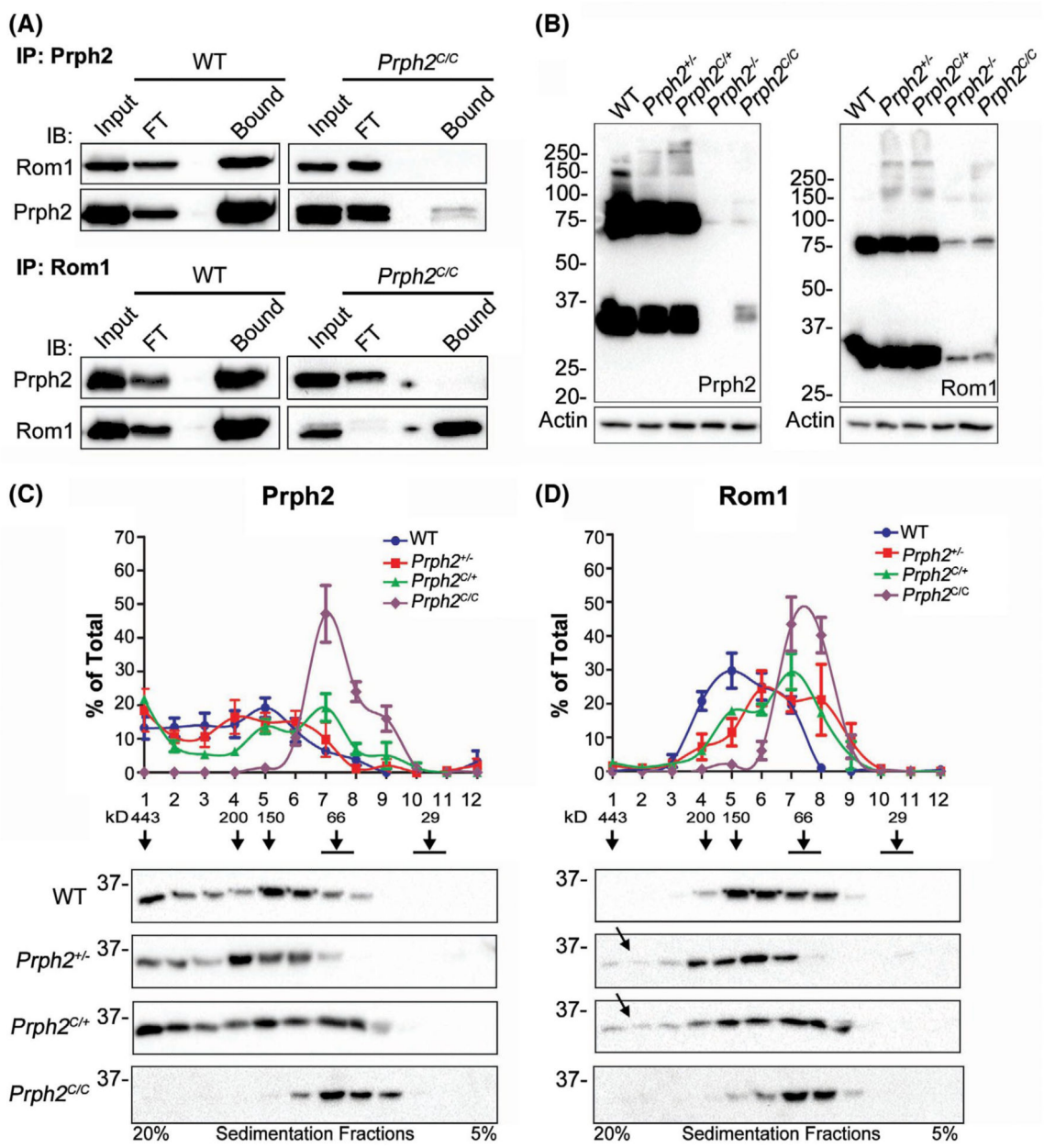

FIGURE 2.

C213Y Prph2 leads to abnormalities in Prph2/Rom1 oligomerization. A, Reciprocal immunoprecipitation with anti-Prph2 (top panel) and anti-Rom1 (bottom panel) antibodies was performed on retinal extracts from P30 WT and *Prph2*$^{C/C}$. B, Nonreducing SDS-PAGE/immunoblots were performed on whole retinal extract in the presence of NEM-containing buffer and were probed with antibodies against Prph2 (left), Rom1 (right), and actin (bottom) as a loading control. C-D, To analyze Prph2/Rom1 complexes, three independent (n = 3) retinal extracts were prepared from each of the indicated genotypes and run on a continuous 5% to 20% nonreducing sucrose gradient. Fractions were collected and analyzed using reducing SDS-PAGE and immunoblotting using antibodies specific for Prph2 (C) and Rom1 (D). The position of standard molecular weight markers is marked above the relevant

fraction as demonstrated previously.[26] Graphs plot mean (±SEM) amount of Prph2/Rom1 in each fraction as a % of total Prph2/Rom1. Arrows in (D) highlight small quantity of higher order Rom1 complexes in mutant retinas

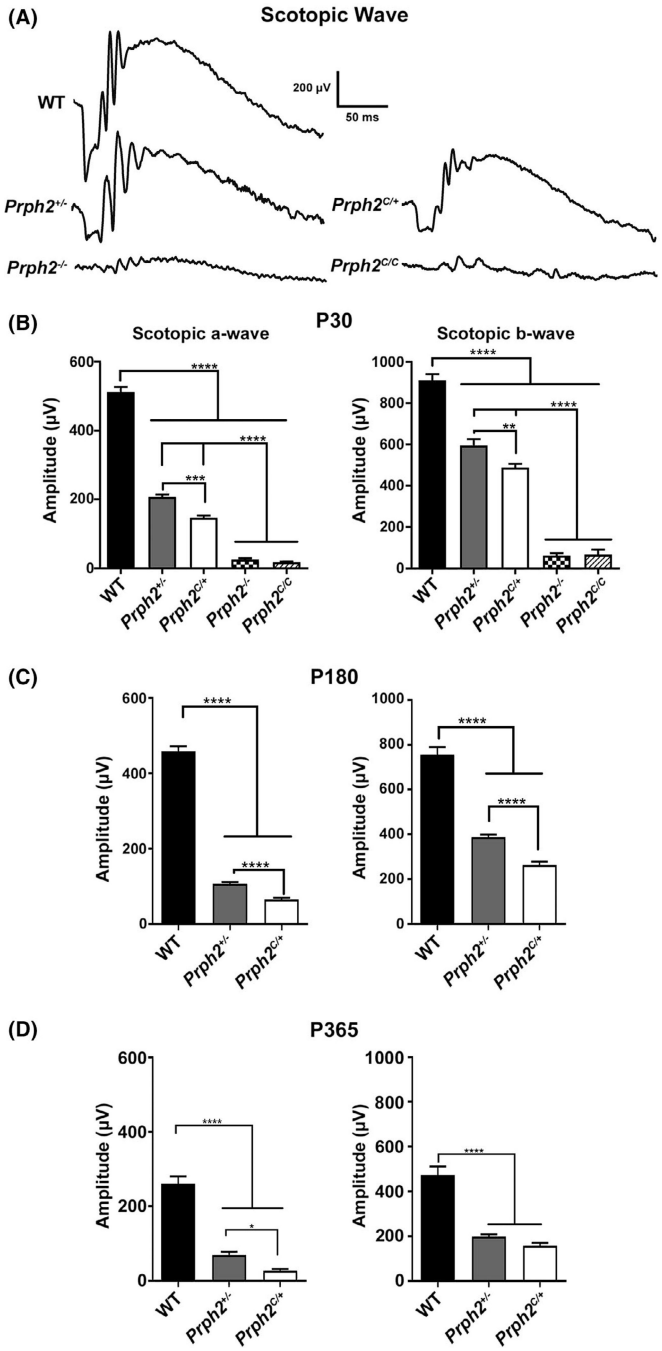

FIGURE 3.

Heterozygous C213Y Prph2 exerts dominant rod functional defect. Full-field ERGs were recorded under scotopic conditions at P30, P180, and P365. Shown are representative ERG wave forms from the indicated genotypes at P30 (A). B-D, Maximum scotopic a- and b-waves are plotted for P30 (B) P180 (C), and P365 (D). Data are presented as mean ± SEM from 5–7 mice per genotype. *$P < .05$, **$P < .01$, ***$P < .001$, and ****$P < .0001$ in one-way ANOVA with ANOVA with Tukey's post-hoc comparison

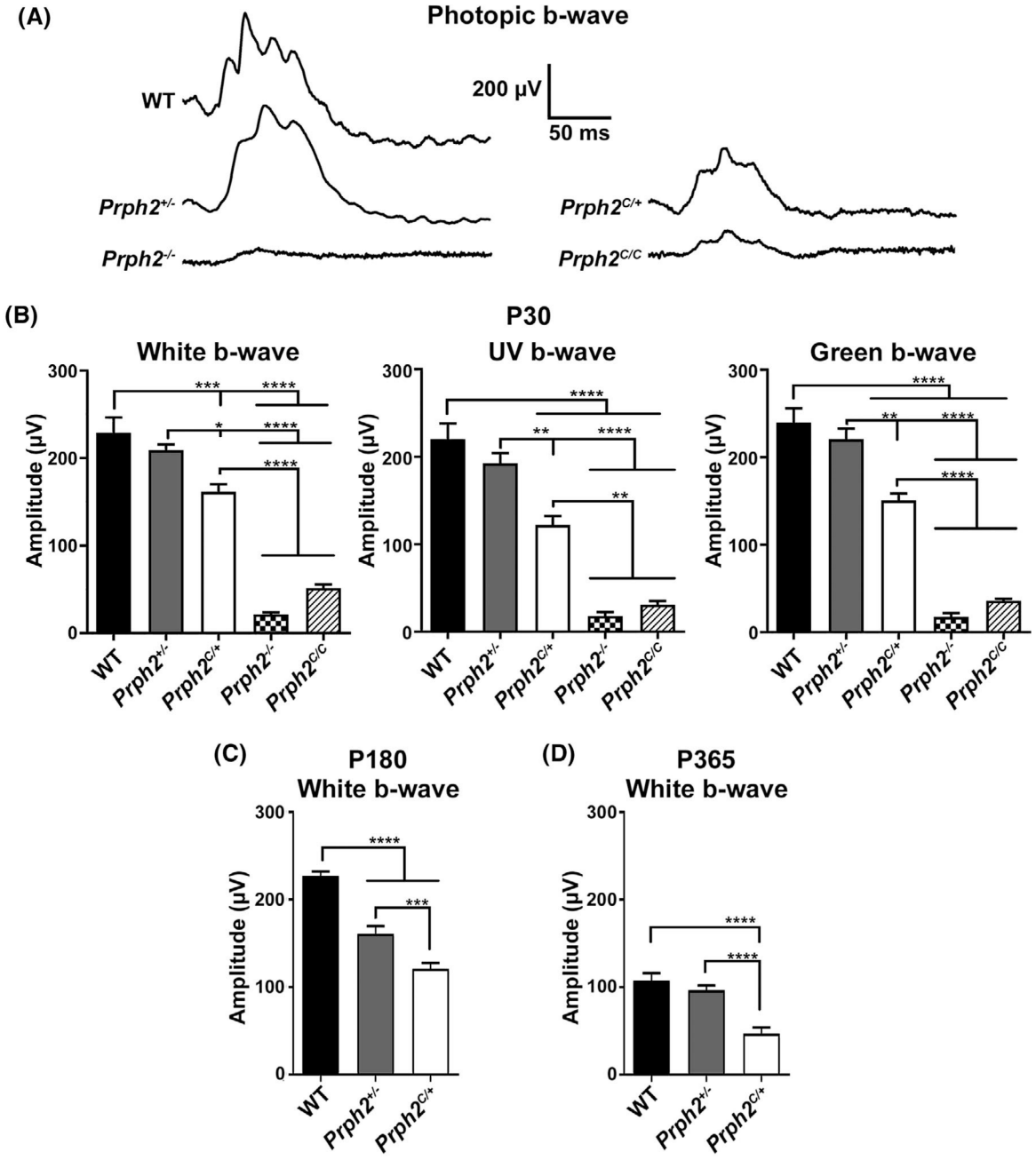

FIGURE 4.

C213Y Prph2 exerts dominant cone functional defect. Full-field ERGs were recorded under photopic conditions (representative waveforms shown in A). B, Maximum amplitudes are shown at P30 recorded in response to white, green, and UV light. Maximum photopic b-wave amplitudes recorded in response to white light at P180 (C) and P365 (D) are plotted. Data are presented as mean ± SEM from 5 to 7 mice per genotype. *$P < .05$, **$P < .01$, ***$P < .001$, and ****$P < .0001$ in one-way ANOVA with ANOVA with Tukey's post-hoc comparison

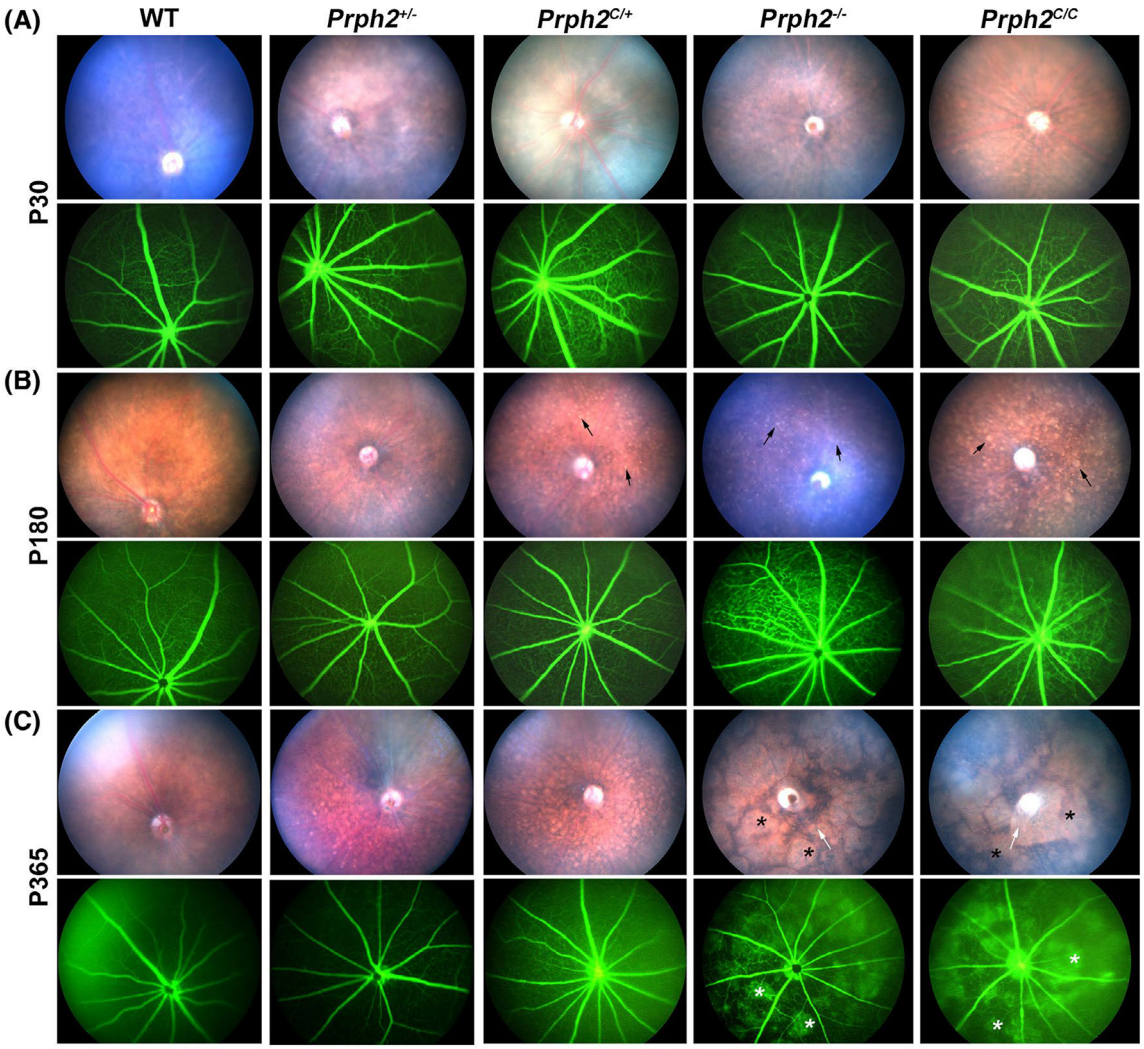

FIGURE 5.

Fundus photographs of *Prph2*$^{C/+}$ show an increase in retinal flecking at P180. Representative fundus images (top) and corresponding fluorescein angiograms (bottom) from the indicated genotypes were performed at P30 (A), P180 (B), and P365 (C). Black arrows denote flecking phenotype found in the *Prph2*$^{C/+}$ as well as the *Prph2*$^{-/-}$, and *Prph2*$^{C/C}$. White arrows point to splotching, likely due to severe photoreceptor degeneration which occurs at later ages. Asterisks denote examples of splotches that align with the leaky vasculature observed in fluorescein angiograms. N = 6–8 eyes/group

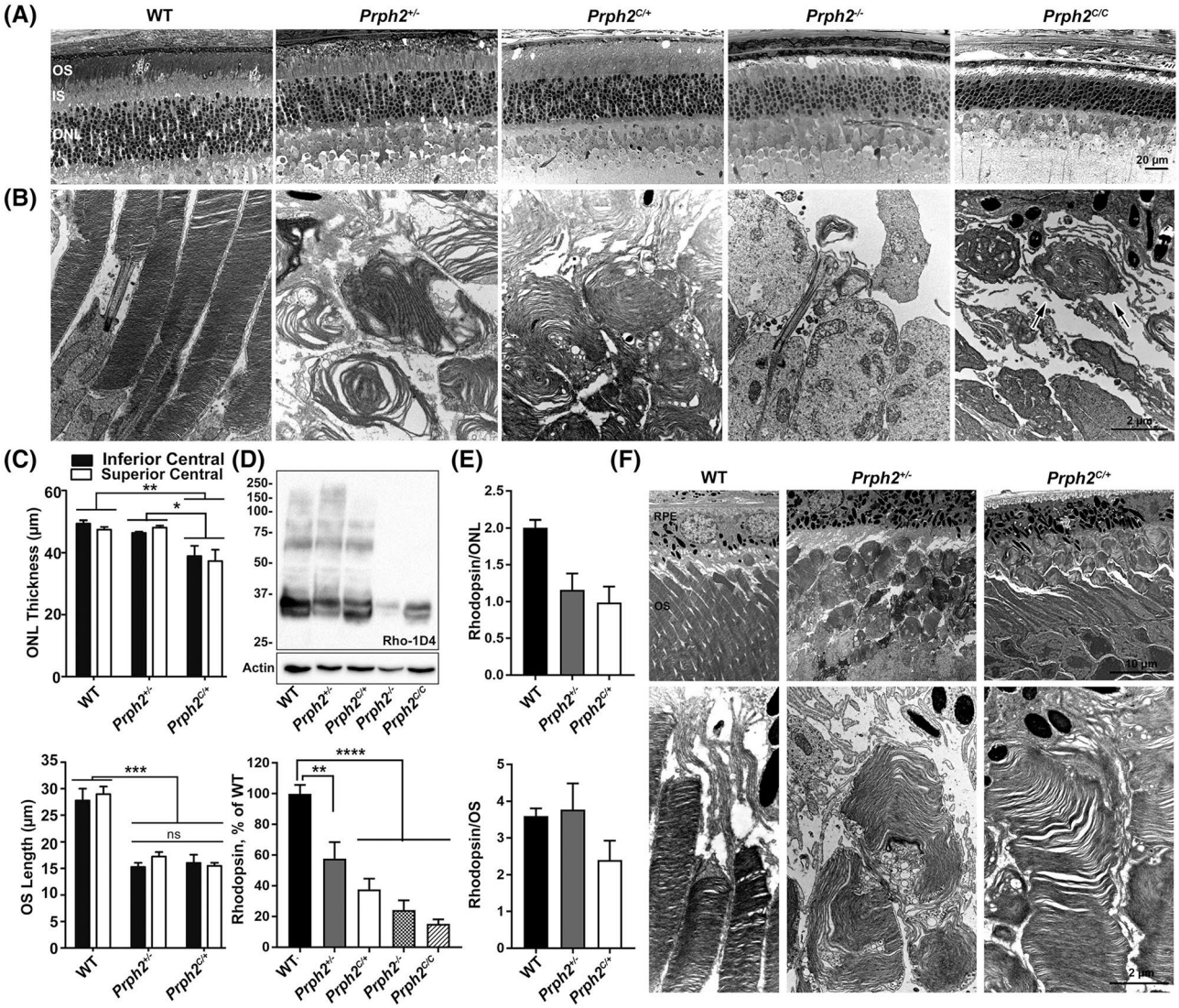

FIGURE 6.

C213Y Prph2 is unable to support proper OS ultrastructure and leads to photoreceptor degeneration. Representative light microscopy (A) and transmission electron microscopy (B) from retinas of the indicated genotypes performed at P30. Arrows show highly malformed OSs in the *Prph2*$^{C/C}$. C, ONL thickness and OS length were measured from the superior and inferior central retina and plotted as a mean ± SEM. D, Rhodopsin protein levels were assessed by immunoblot analysis (top) and quantified densitometrically on non-saturated blots. Graph shows rhodopsin levels normalized to actin and plotted as a % of WT. E, Mean rhodopsin levels are plotted as a ratio to ONL thickness (top) and OS length (bottom). F, Low (upper panels) and high (lower panels) magnification electron microscopy of the indicated genotypes showing improvements on the overall OS structures in the C213Y Prph2 retina in comparison with *Prph2*$^{+/-}$ at P180. Graphs show mean ± SEM. *$P < .05$, **$P < .01$, ***$P < .001$, ****$P < .0001$ by one-way ANOVA (D) or two-way ANOVA (C) with Tukey's post-hoc comparison. N = 3–4 retinas/genotype for histological analyses and 4–8 retinas per genotype for immunoblots. Scale bars: 20 μm (A), 10 μm (F-top), 2 μm (B, F-bottom). IS,

inner segment; ONL, outer nuclear layer; OS, outer segment; RPE, retinal pigment epithelium

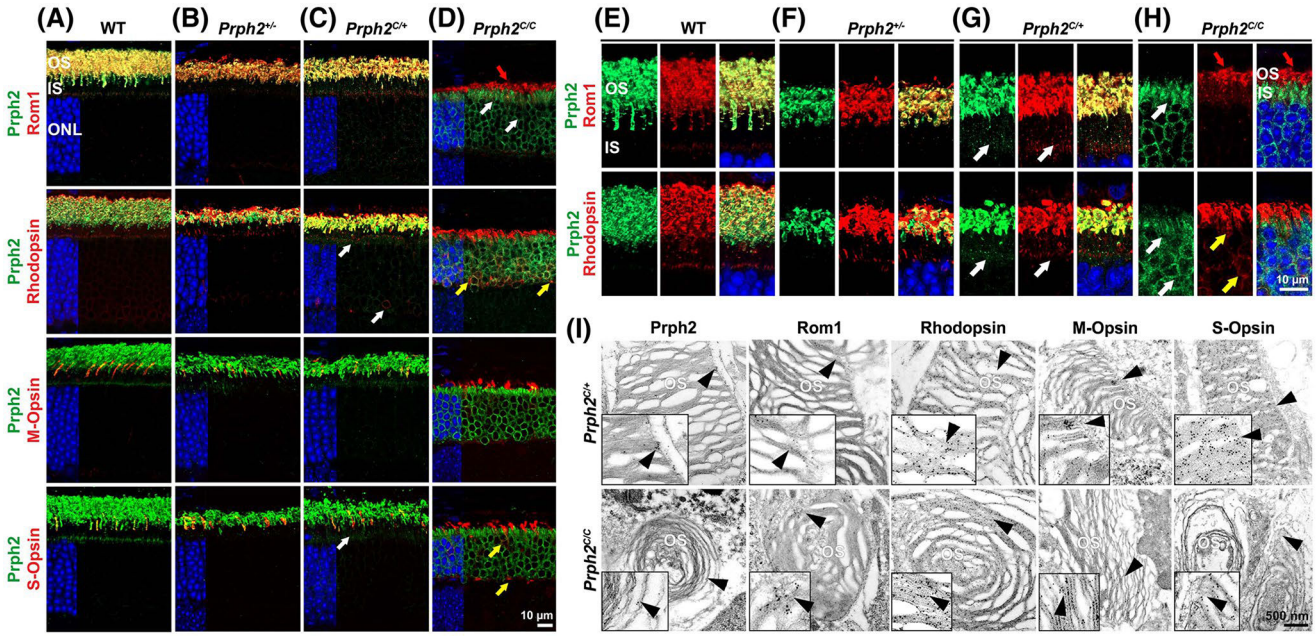

FIGURE 7.

C213Y Prph2 localizes abnormally to the inner segment and outer nuclear layer. A-H, Retinal sections from the indicated genotypes were immunofluorescently co-labeled with Prph2 (green) and Rom1, rhodopsin, S-opsin, and M-opsin (red) at P30. Nuclei in all sections were counterstained with DAPI (blue). White arrows show accumulation of Prph2 in the ONL and IS. Yellow arrows show mislocalization of rhodopsin and S-opsin in the ONL and IS. Red arrows show proper localization of Rom1 to the OS layer in the *Prph2*$^{C/C}$. Panels A-H were captured at 63× with E-H showing enlarged regions from A to D. I, Shown is electron microscopy of retinal sections immunogold labeled for Prph2, Rom1, rhodopsin, S-opsin, and M-opsin at P30. Insets in all images show higher magnifications of the marked areas with black arrowheads. Scale bars: 10 μM (A-H), 500 nm (I). IS, inner segments; ONL, outer nuclear layer; OS, outer segments

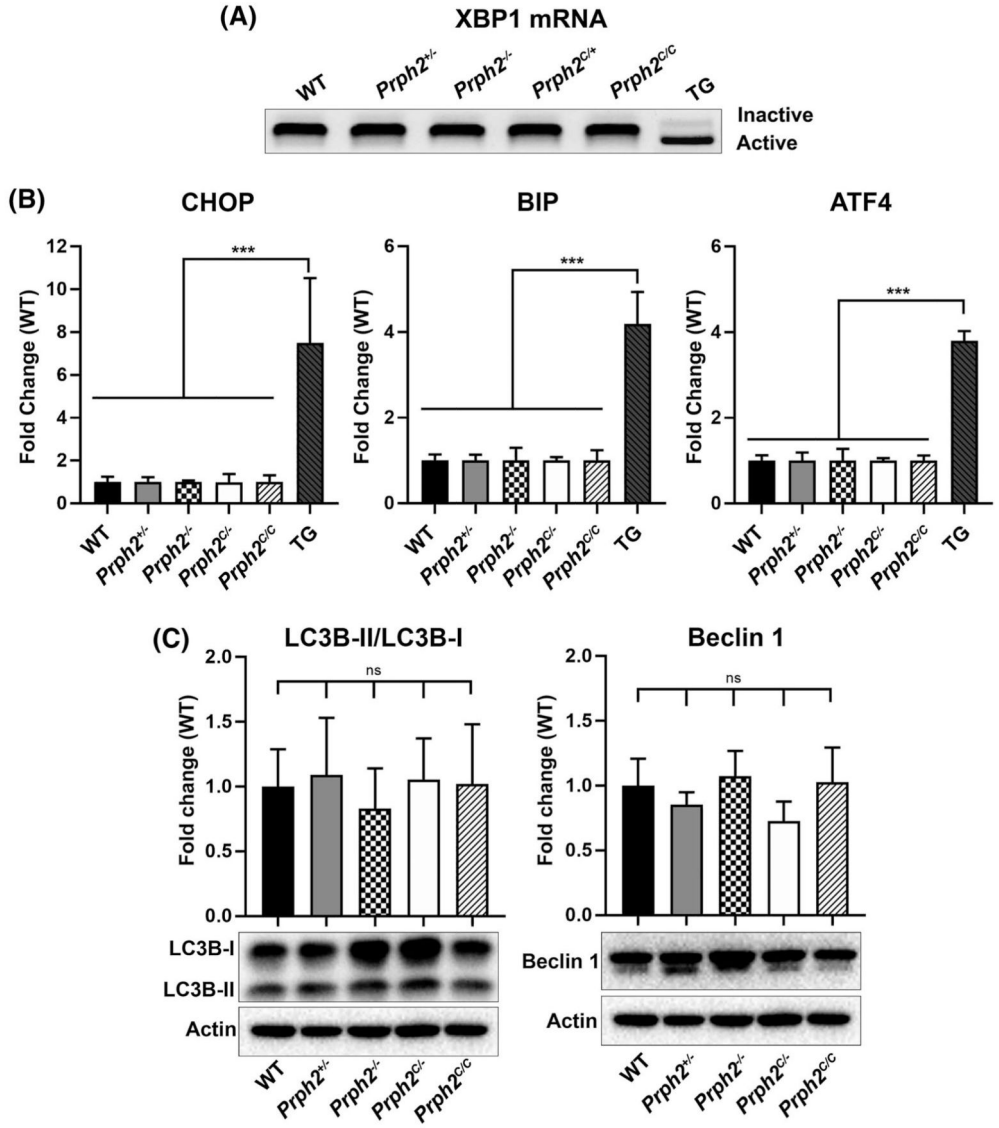

FIGURE 8.

ER stress and autophagy are not implicated in the observed mutant phenotype. A-B, Total mRNA was harvested from three independent retinal extracts per indicated genotypes at P30 and each was tested for XBP1 mRNA cleavage/activation on an agarose gel (A) or underwent by qRT-PCR quantification for the common ER stress markers Activating transcription factor 4 (ATF4), Binding immunoglobulin protein (aka GRP-78) (BIP), and C/EBP homologous binding protein (CHOP) (B). C, Immunoblot was performed to analyze markers of autophagic flux through the LC3B-II/I ratio and Beclin 1 expression from three independent samples per genotype. Plotted are mean ± SEM. *** $P < .001$ by one-way ANOVA with Tukey's post-hoc comparison: ns, not significant

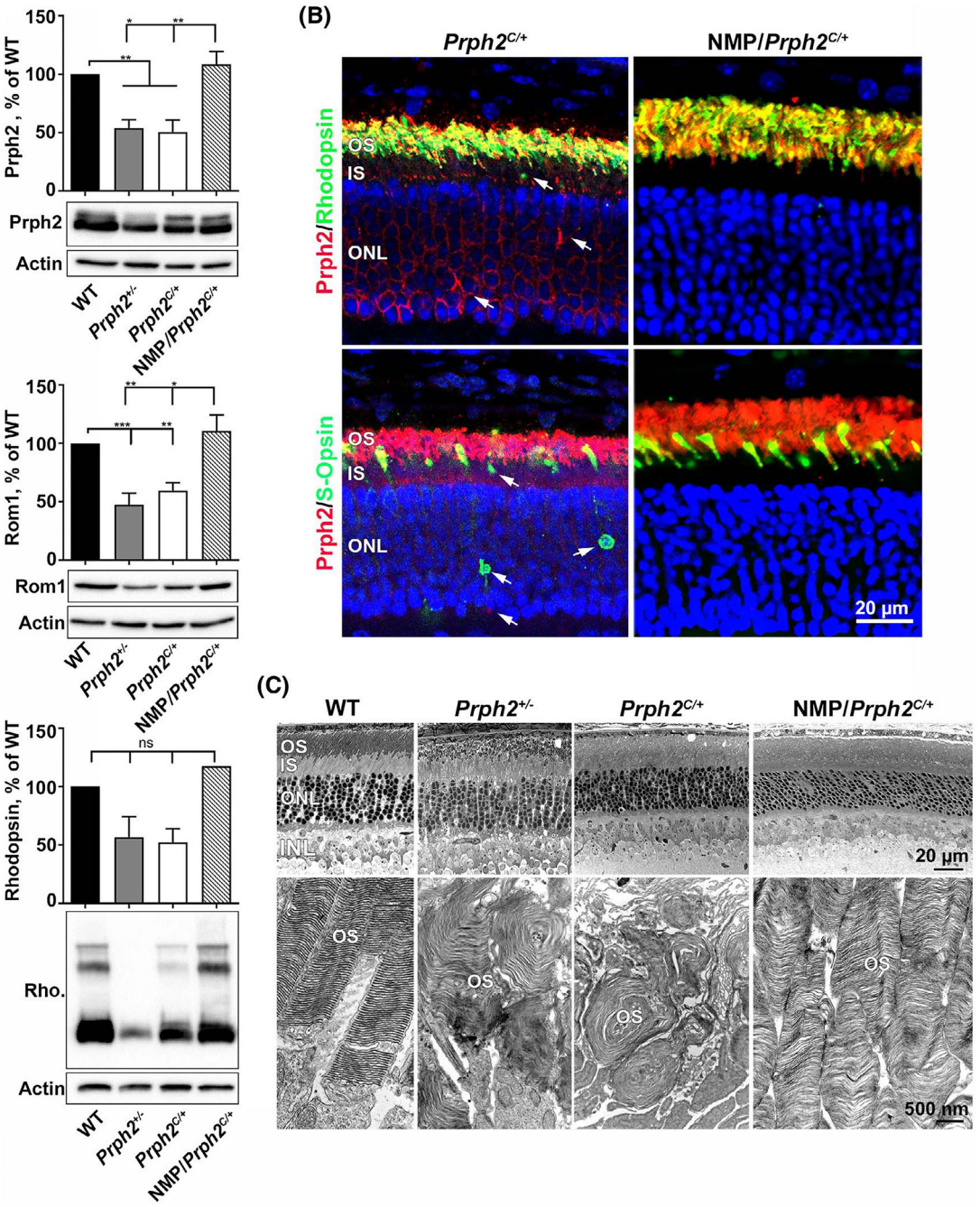

FIGURE 9.

WT Prph2 supplementation improves cellular phenotypes in the *Prph2*$^{C/+}$. A, Shown are immunoblots and associated densitometric analysis of Prph2, Rom1, and rhodopsin relative to actin as a loading control from retinal extracts collected at P30. B, P30 retinal sections were immunofluorescently labeled for Prph2 (red) and rhodopsin or S-opsin (green). Nuclei are counterstained with DAPI (blue). Prph2 and S-opsin are mislocalized to the inner segment and outer nuclear layer of *Prph2*$^{C/+}$ (white arrows) but properly localized to the OS in NMP/*Prph2*$^{C/+}$ retinas. Immunofluorescence experiments were repeated three times using

sections from 3–5 different animals. C, Light microscopy (upper) and electron microscopy (lower) taken from P30 retinas of the indicated genotypes. Scale bars: 20 μm (B, C-top) and 500 nm (C-bottom). INL, inner nuclear layer; IS, inner segment; ONL, outer nuclear layer; OS, outer segment. *$P < .05$, **$P < .01$, and ***$P < .001$ by one-way ANOVA with Tukey's post-hoc comparison

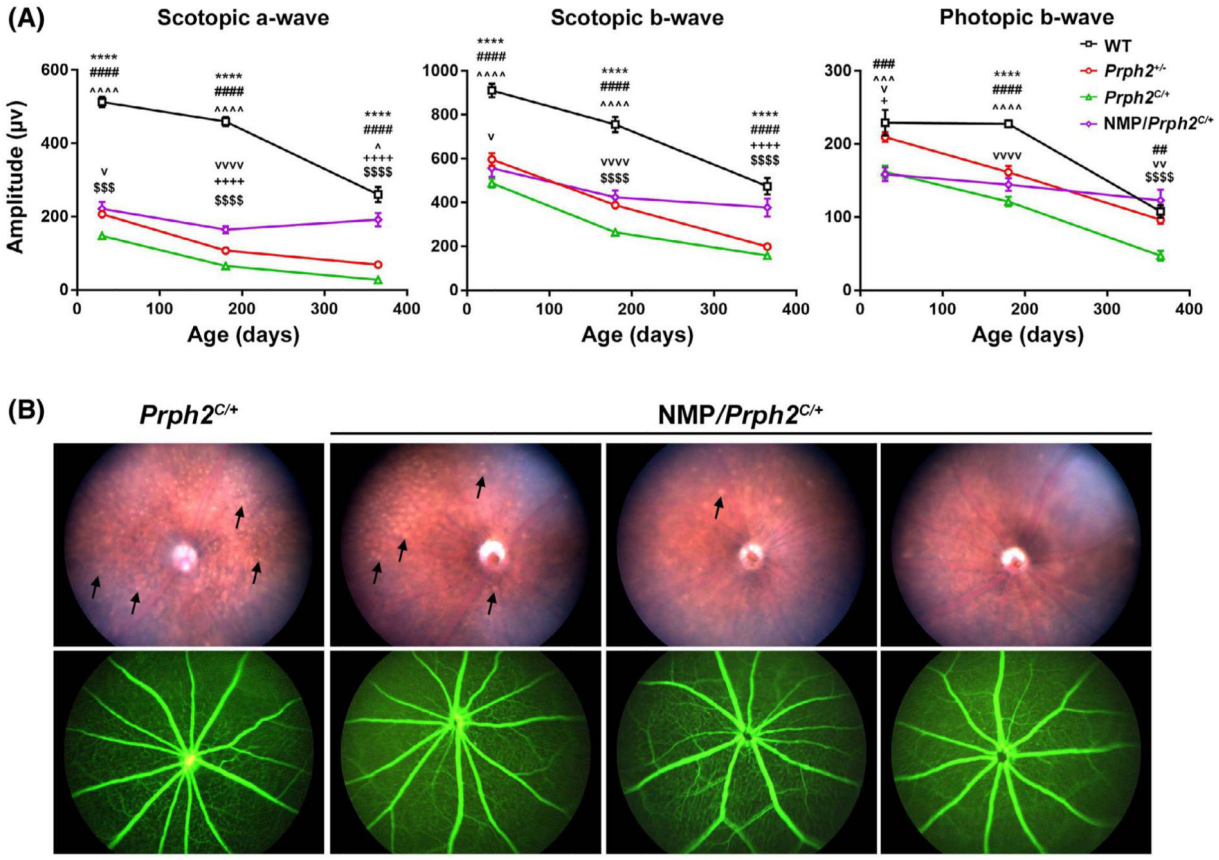

FIGURE 10.

WT Prph2 supplementation does not rescue rod or cone function in the *Prph2*$^{C/+}$. A, Full-field ERGs were recorded under scotopic or photopic conditions at P30, P180, and P365 from the indicated genotypes. Plotted are mean (±SEM) maximum scotopic a-, scotopic b-, and photopic b- wave amplitudes. N = 5–15 animals/genotype/age. Each symbol represents a different pairwise comparison: * WT vs. *Prph2*$^{+/-}$, # WT vs. *Prph2*$^{C/+}$, ^ WT vs. NMP/*Prph2*$^{C/+}$, v *Prph2*$^{+/-}$ vs. *Prph2*$^{C/+}$, + *Prph2*$^{+/-}$ vs. NMP/*Prph2*$^{C/+}$, and $ *Prph2*$^{C/+}$ vs. NMP/*Prph2*$^{C/+}$. One symbol $P < .05$, two symbols $P < .01$, three symbols $P < .001$ and four symbols $P < .0001$ by one-way ANOVA with Tukey's post-hoc comparison. B, Shown are representative fundus images (top) and fluorescein angiograms (bottom) from animals of the indicated genotypes captured at P180

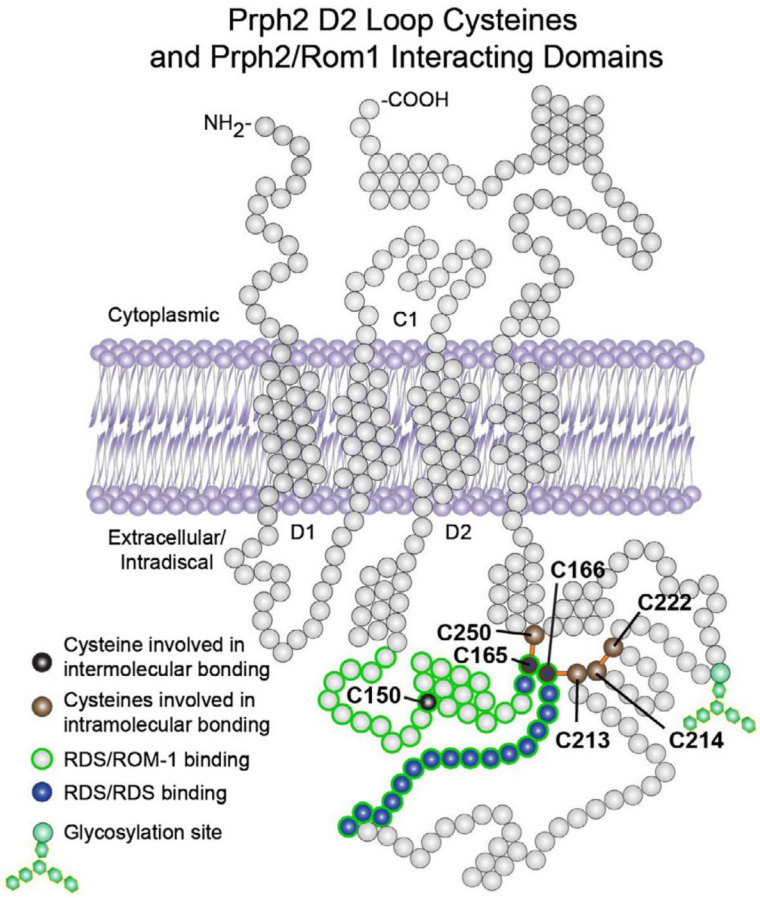

FIGURE 11.

Cysteines are essential for the organization of the Prph2 D2 loop. Shown is a diagram highlighting the seven conserved D2 loop cysteines in Prph2 and their position with regard to the location of the Prph2/Rom1 interaction domains

TABLE 1

Antibodies used for immunofluorescence (IF), immunogold (IGL), and western blotting (WB)

Antigen	Antibody	Species	Use	Source	References
Prph2	RDS-CT	Rbt-PC	WB, IF	In house	(16,26)
Prph2	mAB 2B7	Ms-MC	WB, IF	In house	(46,61)
Prph2	MPCT	Rbt-PC	IGL	Dr Andrew Goldberg	
Rom1	ROM1-CT	Rbt-PC	WB, IF	In-house	(16,26)
Rom1	mAB 2H5	Ms-MC	WB, IF	In-house	(46,62)
Rhodopsin	mAB 1D4	Ms-MC	WB, IF	Dr Robert Molday	(63,64)
Rhodopsin	Bov.Opsin	Rbt-PC	IGL	Dr Steve Fliesler	(16,18)
S-opsin	S-opsin	Rbt-PC	WB, IF	In-house	(29)
S-opsin	OPN1SW (N-2)	Gt-PC	IF	Santa Cruz Biotechnology, cat# sc-14363	(18)
S-opsin	Craft S-opsin	Rbt-PC	IGL	Dr Cheryl Craft	(18,27)
M-opsin	Opsin 1 (Medium Wave)	Rbt-PC	WB, IF	Novus Biologicals cat# 110–74730	
M-opsin	Craft M-opsin	Rbt-PC	IGL	Dr Cheryl Craft	
Actin-HRP	Clone AC-15	Ms-MC	WB	Sigma Aldrich, cat# A3854	(15,18)
Beclin 1	Beclin 1	Rbt-PC	WB	Abcam, ab62557	
LC3B	LC3B	Rbt-PC	WB	Abcam, ab51520	

Abbreviations: Gt-PC, goat polyclonal; Ms-MC, mouse monoclonal; Rbt-PC, rabbit polyclonal.

TABLE 2

Primers for qRT-PCR

qRT-PCR Primers		
Gene	**Sequence 5′–3′**	**F/R**
Atf4	GGACAGATTGGATGTTGGAGAAAATG	F
Atf4	GGAGATGGCCAATTGGGTTCAC	R
BIP	GTTTGCTGAGGAAGACAAAAAGCTC	F
BIP	CACTTCCATAGAGTTTGCTGATAAT	R
CHOP	GTCCAGCTGGGAGCTGGAAG	F
CHOP	CTGACTGGAATCTGGAGAG	R
XBP1	GAACCAGGAGTTAAGAACACG	F
XBP1	AGGCAACAGTGTCAGAGTCC	R
Hprt	GCAAACTTTGCTTTCCCTGGTT	F
Hprt	CAAGGGCATATCCAACAACA	R
Prph2	GTTCAAGTGCTGTGGGAACA	F
Prph2	CTGTGTGGAGGTAGCGGAGT	R

Abbreviations: Atf4, activating transcription factor 4; BIP, binding immunoglobulin protein (aka GRP-78); CHOP, C/EBP homologous binding protein; Hprt, hypoxanthine phosphoribosyltransferase; Prph2, peripherin/rds; XBP1, X-box binding protein.